Title

FOXO1 promotes endothelial cell elongation and angiogenesis by up-regulating the phosphorylation of myosin light chain 2

Authors

Kiyomi Tsuji-Tamura[1],* and Minetaro Ogawa [2]

Affiliations

[1]Oral Biochemistry and Molecular Biology, Department of Oral Health Science, Faculty of Dental Medicine and Graduate School of Dental Medicine, Hokkaido University, Kita 13, Nishi 7, Kita-Ku, Sapporo, 060-8586, Japan

[2]Department of Cell Differentiation, Institute of Molecular Embryology and Genetics, Kumamoto University, 2-2-1 Honjo, Chuo-Ku, Kumamoto, 860-0811, Japan

*Author for correspondence: Kiyomi Tsuji-Tamura, Oral Biochemistry and Molecular Biology, Department of Oral Health Science, Faculty of Dental Medicine and Graduate School of Dental Medicine, Hokkaido University, Kita 13, Nishi 7, Kita-Ku, Sapporo 060-8586, Japan, Tel: +81-11-706-4234, e-mail: ktamuratsuji@den.hokudai.ac.jp, ORCID ID: 0000-0002-0961-5402

Types of paper: Original Article

Abstract

The forkhead box O1 (FOXO1) is an important transcription factor related to proliferation, metabolism, and homeostasis, while the major phenotype of FOXO1-null mice is abnormal vascular morphology, such as vessel enlargement and dilation. In *in vitro* mouse embryonic stem cell (ESC)-differentiation system, *Foxo1*$^{-/-}$ vascular endothelial cells (ECs) fail to elongate, and mimic the abnormalities of FOXO1-deficiency *in vivo*. Here, we identified the *PPP1R14C* gene as the FOXO1 target genes responsible for elongating using transcriptome analyses in ESC-derived ECs (ESC-ECs), and found that the FOXO1-PPP1R14C-myosin light chain 2 (MLC2) axis is required for EC elongation during angiogenesis. MLC2 is phosphorylated by MLC kinase (MLCK) and dephosphorylated by MLC phosphatase (MLCP). PPP1R14C is an inhibitor of PP1, the catalytic subunit of MLCP. The abnormal morphology of *Foxo1*$^{-/-}$ ESC-ECs was associated with low level of PPP1R14C and loss of MLC2 phosphorylation, which were reversed by PPP1R14C-introduction. Knockdown of either FOXO1 or PPP1R14C suppressed vascular cord formation and reduced MLC2 phosphorylation in human ECs (HUVECs). The mouse and human PPP1R14C locus possesses an enhancer element containing conserved FOXO1-binding motifs. *In vivo* chemical inhibition of MLC2 phosphorylation caused dilated vascular structures in mouse embryos. Furthermore, *foxo1* or *ppp1r14c*-knockdown zebrafish exhibited vascular malformations, which were also restored by PPP1R14C-introduction. Mechanistically, FOXO1 suppressed MLCP activity by up-regulating *PPP1R14C* expression, thereby promoting MLC2 phosphorylation and EC elongation, which are necessary for vascular development. Given the importance of MLC2 phosphorylation in cell morphogenesis, this study may provide novel insights into the role of FOXO1 in control of angiogenesis.

Keywords: Angiogenesis, endothelial cells, elongation, FOXO1, MLC, PPP1R14C

Introduction

Forkhead box O1 (FOXO1, also known as FKHR) is a pleiotropic transcription factor that is involved in diverse cellular processes, including cell proliferation, metabolism, and homeostasis (for reviews, see [1][2]). FOXO1 has also been implicated in various pathological conditions, including retinopathy, diabetes, atherosclerosis, and cancer [3] [4] (for reviews, see [5] [6]). Angiogenesis has been identified as the cause of or an aggravating factor in these diseases. However, the role of FOXO1 in angiogenesis has not yet been elucidated in detail.

Foxo1-deficient mouse lines exhibited embryonic lethality due to severe defects in vascular morphology, such as enlarged yolk sac vessels, dilated capillary beds in the head, and hypoplasia of the dorsal aorta [7] [8]. Vascular endothelial cell (EC)-specific deletion of *Foxo1* recapitulated the phenotype of *Foxo1*-null mice [9] [10]. Systemic and EC-specific *Foxo1*-deficient embryos possessed intact differentiated ECs, suggesting generally normal growth and differentiation of ECs, but exhibited defective angiogenic remodeling. Therefore, FOXO1 may play an essential role in the morphological regulation of ECs, which may not be predicted from its known functions, such as cell proliferation and metabolism.

The role of FOXO1 in angiogenesis has been examined using cultured ECs. The knockdown of *FOXO1* in human

umbilical vein ECs (HUVECs) enhanced EC migration, and increased tube lengths in a matrigel culture [11]. FOXO1 was also found to suppress c-MYC signaling, which a critical regulator of cell proliferation and metabolism [12]. These findings suggested the anti-angiogenic functions of FOXO1. In contrast, other studies reported a pro-angiogenic role for FOXO1. *FOXO1*-knockdown in HUVECs induced G1 cell-cycle arrest, and inhibited migration and proliferation [10], and caused loss of cell polarity in the directional migration [3]. Unfortunately, none of these *FOXO1*-knockdown HUVECs mimicked the dilated vascular structure of Foxo1-null mice [11] [3] [9] [10]. Therefore, the function of FOXO1 in angiogenesis has remained controversial and elusive. FOXO1 exerts its functions in an environmental condition-dependent manner [13] (for a review, see [14]). It is necessary to use an *in vitro* model that recapitulates the *in vivo* critical phenotypes of ECs.

Mouse embryonic stem cells (ESCs) differentiate into ECs by passing through the mesodermal stage [15]. ESC-derived ECs (ESC-ECs) exhibit a flagstone-like morphology in the co-culture system with OP9 stromal cells. When stimulated with vascular endothelial growth factor (VEGF), a strong angiogenesis inducer, ESC-EC morphology shifts from flagstone to elongated in co-culture system, and furthermore generated a vessel-like structure with thin and long endothelial sprouts in 3D spheroid culture [16]. We previously reported that *Foxo1*$^{-/-}$ ESC-ECs failed to take the normal elongated morphology in the co-culture system [7][17], and generated an abnormal vessel-like structure with thick and short endothelial sprouts in 3D spheroid culture [18] [19] [20] [21]. Namely *Foxo1*$^{-/-}$ ESC-ECs mimicked the phenotype of the dilated vessels in *in vivo* deficiency of *Foxo1*. Therefore, ESC differentiation systems provide a promising model for EC morphology during angiogenesis.

The interaction of actin cytoskeleton and myosin motor proteins has been reported not only in muscle contraction, but also in a number of non-muscle cell events, including cell migration, adhesion, polarization, and division (for reviews, see [22] [23]). Myosin II is a hexameric protein consisting of two myosin heavy chains and two pairs of essential myosin light chains (MLC1, also known as ELC) and regulatory myosin light chains (MLC2, also known as RLC). Myosin II changes its structure and slides along actin filaments in an ATP-dependent manner, thereby generating tension. This process is also regulated by the phosphorylation of MLC2, which is induced by myosin light chain kinase (MLCK) in a calcium/calmodulin-dependent manner [24] (for a review, see [25]). The actin-myosin interaction plays a vital role in endothelial barrier function, vascular permeability, and angiogenesis [26] [27] [28] [29] (for a review, see [30]). We previously reported that the abnormal morphology of *Foxo1*$^{-/-}$ ESC-ECs was associated with the disordered distribution of the actin cytoskeleton [18] [19] [20].

In the present study, we investigated the role of FOXO1 in angiogenesis, and the molecular mechanisms in EC morphogenesis using an *in vitro* angiogenesis model of mouse ESC-ECs and human ECs and *in vivo* vascular analysis of mouse and zebrafish embryos. We identified the protein phosphatase 1, regulatory inhibitor subunit 14C (*Ppp1r14c,* also known as *Kepi*) gene as a downstream target of FOXO1, and found that the FOXO1-PPP1R14C-MLC2 axis was required for EC elongation during angiogenesis.

Materials and Methods

Cells

The *Foxo1*$^{-/-}$ mouse ESC line and parental *Foxo1*$^{+/+}$ ESC line were described previously [7]. The EGFP-F/*Foxo1*$^{-/-}$ ESC line [19] is a subclone of the *Foxo1*$^{-/-}$ ESC line that constitutively expresses a farnesylated enhanced green fluorescent protein (EGFP). The F10-EGFP ESC line [19] [31] is a subclone of the wild-type KTPU8 ESC line [32] that expresses EGFP under the control of the EC-specific F10-44 enhancer of the *Mef2c* gene [33]. OP9 stromal cells [34] were used as feeder cells for ESC differentiation. The ESC lines and OP9 cells were maintained as previously reported [18]. The UV2 (RCB1994, RIKEN BRC, Tsukuba, Japan) and bEnd.3 (CRL-2299, ATCC, Manassas, VA, USA) mouse EC lines were cultured in Dulbecco's modified minimum essential medium (Wako Pure Chemical Industries, Osaka, Japan) supplemented with 10% fetal bovine serum (FBS). HUVECs (C2519A, Lonza, MD USA) were cultured on gelatin-coated plates using the Endothelial Cell Growth Medium Kit (C-22110, Takara Bio Inc., Shiga, Japan) and used in experiments between passage numbers three and seven.

Animals

Experiments using animals were approved by the Animal Care and Use Committee of Kumamoto University (No. A27-001) and the Committee on Animal Experimentation of Hokkaido University (No. 21-0078), and were conducted according to institutional guidelines consistent with the Guidelines for Proper Conduct of Animal Experiments (Science Council of Japan, June 1, 2006) and the Law for the Humane Treatment and Management of Animals (Law No. 105, 1973) in Japan. Pregnant ICR mice were provided by Kyudo Co., Ltd. (Saga, Japan) and Japan SLC (Shizuoka, Japan). Mice were euthanized by cervical dislocation according to the guidelines for the euthanasia of animals of the American Veterinary Medical Association (AVMA, https://www.avma.org/). Transgenic zebrafish *Tg(fli1a:Myr-mCherry)*^{ncv1} [35] were obtained from the National Bioresource Project. Adult zebrafish were maintained at 28°C with a 14-h light:10-h dark cycle. Fertilized zebrafish eggs were obtained by breeding, cultured in the breeding water, E3 solution (5 mM NaCl, 0.17 mM KCl, 0.33 mM $CaCl_2$, and 0.33 mM $MgSO_4$, pH7.4), and maintained at 28°C [36] (for a book, see [37]).

Antibodies and chemical inhibitors

An anti-mouse VE-cadherin rat monoclonal antibody (mAb) (VECD1) [38] and anti-mouse Flk1 rat mAb (Avas12) [39] were purified and fluorescently labeled as previously reported [20]. A phycoerythrin-conjugated anti-mouse CD31 rat mAb (102408, Biolegend, San Diego, CA, USA), anti-phospho-MLC2 (Ser19) mouse mAb (3675, Cell Signaling, Beverly, MA, USA), Alexa Fluor 488-conjugated phalloidin (A12379, Invitrogen, Carlsbad, CA, USA), FITC-conjugated isolectin B4 (IB4) (L2895, Sigma-Aldrich), and anti-Type IV collagen rabbit polyclonal antibody (pAb) (2150-1470, AbD Serotec, Oxford, UK) were commercially obtained. Tautomycetin (2305, Tocris Bioscience, Ellisville, MS, USA), ML7 hydrochloride (ML7) (4310, R&D System, Inc., Minneapolis, MN, USA), and Okadaic acid (O7885, Sigma-Aldrich) were commercially obtained.

DNA microarray data analysis

Our previous DNA microarray data (NCBI GEO accession No. GSE76366) [19] were analyzed to detect the genes responsible for VEGF-A165-induced FOXO1-dependent EC elongation. The online tool GEO2R (https://www.ncbi.nlm.nih.gov/geo/geo2r/) extracted differentially expressed genes (DEGs) by comparing the four groups of ECs derived from *Foxo1*$^{+/+}$ and *Foxo1*$^{-/-}$ ESCs in the absence or presence of a stimulation with 10 ng/ml

VEGF-A165. DEGs were sorted using a criterion based on a log2 fold-change (LogFC) <-0.6. A gene ontology (GO) enrichment analysis of these DEGs was performed by the functional annotation tool DAVID (https://david.ncifcrf.gov/summary.jsp), using gene counts >20 and a *P*-value <0.001 as thresholds.

ESC differentiation and FACS

ESCs were cultured on an OP9 cell layer in alpha-MEM (Invitrogen) supplemented with 10% FBS and 50 μM 2-mercaptoethanol (induction medium). After 3.5–4.5 days or 6–7 days of culture, $Flk1^+$ mesodermal cells or VE-$cadherin^+$ $CD31^+$ ECs, respectively, were purified using a Special Order FACSAria II cell sorter (BD Bioscience, San Jose, CA, USA) as previously reported [18] [20].

Quantitative real-time PCR and conventional PCR

Total RNA was extracted using a RNeasy Plus Mini Kit (Qiagen, Hilden, Germany) or QIAzol lysis reagent (Qiagen) and reverse-transcribed using the Omniscript Reverse Transcription kit (Qiagen) in a mixture consisting of oligo (dT) primers and random primers. Quantitative real-time PCR was performed using the TaqMan Universal PCR Master Mix (Applied Biosystems, Foster city, CA, USA) for the Applied Biosystems 7300 real-time PCR system (Applied Biosystems) or QuantiTect SYBR Green PCR kit (Qiagen) for the StepOne real-time PCR system (Applied Biosystems). Conventional PCR to detect gene expression was performed using a Taq PCR Core Kit (Qiagen) and standard thermal cycler (ASTEC PC707, Japan). PCR products were separated on 1.5% agarose gels and visualized with the SYBR Gold Nucleic Acid Gel Stain (Thermo Fisher Scientific) under a UV transilluminator (Red Imaging System, Alpha Innotech, San Diego, CA, USA). The primers used for PCR are described below.

Primers for quantitative real-time PCR

The following primers and/or probes were used: mouse *Foxo1* forward (fwd) 5'-CTACGAGTGGATGGTGAAGAGC-3', reverse (rev) 5'-GGACAGATTGTGGCGAATTGAA-3' and probe 5'-CCGAGCTGTTGCTGTCGCCCTTATCC-3'; mouse *Ppp1r14c* fwd 5'-GAAATTACAGGAAGCTCTCGTAGA-3', rev 5'-CTCTTCTTCTGCGGAGGGC-3' and probe 5'-CTTCCTCATGCCTCTTATCCGGGAGAGC-3'; mouse b2 microglobulin (*B2m*) fwd 5'-GGTCTTTCTGGTGCTTGTCTCA-3', rev 5'-GTTCGGCTTCCCATTCTCCG-3' and probe 5'-ACCGGCCTGTATGCTATCCAGAAAACCC-3'; human *FOXO1* fwd 5'-GCTTCCCACACAGTGTCAAG-3' and rev 5'- TGCTTCTCTCAGTTCCTGCT-3'; human *PPP1R14C* fwd 5'-TCTTGATGCAGACAGTGATGAA-3' and rev 5'-GCCTCTTATCCGAGAAAGCA-3'; human *FOXO3* fwd 5'- AGTCTCCCATGCAGACCATC-3' and rev 5'- AGAGTCCGAAGTGAGCAGGTC-3'; human *RHOA* fed 5'- CAGAAAAGTGGACCCCAGAA-3' and rev 5'- TGCCTTCTTCAGGTTTCACC-3'; human *ACTB* fwd 5'-AGAGCTACGAGCTGCCTGAC-3' and rev 5'-AGCACTGTGTTGGCGTACAG-3'; zebrafish *ppp1r14c* fwd 5'-ACAGTGAAGACGAGAGAGCC-3' and rev 5'-TTCCTCTTATCCTGCCGAGC-3'; zebrafish *actb1* fwd 5'-CCCTGAATCCCAAAGCCAAC-3' and rev 5'-TACAGAGAGAGCACAGCCTG-3'; mouse *Foxo1* fwd 5'-AAGAGCGTGCCCTACTTCAA-3' and rev 5'-TGCTGTGAAGGGACAGATTG-3' (Supplementary Fig. 6a); human *PPP1R14C* fwd 5'-ACGGGTTTTCTTCCAAAGC-3' and rev 5'- CTGCTGTTGCTGCTGAACCT-3' (Supplementary Fig. 6b).

Primers for conventional PCR

The following primers were used: mouse *Foxo1* fwd 5'-AAGAGCGTGCCCTACTTCAA-3'and rev 5'-CCTGCTCTGTCATGATGGGA-3'; mouse *Ppp1r14c* fwd 5'-GTCTTCTTCCAGAGTCCCCG-3' and rev 5'-GCAGTCTACGAGAGCTTCCT-3'; mouse *Ppp1ca* fwd 5'-CAGCTCCCAACTACTGTGGA-3' and rev 5'-CTGAACTGCCCATACTTGCC-3'; mouse *Ppp1cb* fwd 5'-GTGTGCTAGCATCAATCGCA-3' and rev 5'-TCCATAGATTGTAGGTCTGGTGA-3'; mouse *Ppp1cc* fwd 5'-CTCGGGGACTATGTGGACAG-3' and rev 5'-TGTGAACGTTTTCCACAGCT-3'; mouse *Mylk* fwd 5'-CCCCAAGACACCCACAAAAG-3' and rev 5'-CCACTTTCCCAAACAGCTCC-3'; mouse *B2m* fwd 5'-CTGACCGGCCTGTATGCTAT-3' and rev 5'-CCGTTCTTCAGCATTTGGAT-3'; zebrafish *foxo1a* fwd 5'-CTCCATGGACAACAACAGCA-3' and rev 5'-ATTGCTGTGGGAGTTCGGA-3'; zebrafish *foxo1b* fwd 5'- AGCAAGTTCACAAAGAGCCG-3' and rev 5'-GGCACTTCCTGTAGTCCTGT-3'; zebrafish *ppp1r14c* fwd 5'-ACAGTGAAGACGAGAGAGCC-3' and rev 5'-TTCCTCTTATCCTGCCGAGC-3'; zebrafish *ppp1caa* fwd 5'-GCTCCTAACTACTGTGGCGA-3' and rev 5'-TCCTCCTCCACCGTAGTACA-3'; zebrafish *ppp1cab* fwd 5'-AGAGGCAGTTAGTCACGCTT-3' and rev 5'-CGCCATATGACAGCACCTTC-3'; zebrafish *ppp1cb* fwd 5'-TGGGGAGAGAATGATCGTGG-3' and rev 5'-AATTCACCCCGCTGTACTGA -3'; zebrafish *ppp1cc* fwd 5'-CCTGCACAAACATGACCTGG-3' and rev 5'-TGGAAAGAGCACATGAGGGT-3'; zebrafish *mylka* fwd 5'-CTTCTACCCCGACCACAGAG-3' and rev 5'-AGAATCACCTCCTGACCTGC-3'; zebrafish *mylkb* fwd 5'-CAGCTTCGCCTCTGTCATTC-3' and rev 5'-GCCGTCCTCCTCATAGTCAA-3'; zebrafish *actb1* fwd 5'-CCCTGAATCCCAAAGCCAAC-3' and rev 5'-TACAGAGAGAGCACAGCCTG-3'.

Plasmid construction and transfection

The pCAGIPuro vector, carrying a CAG promoter, an IRES, and the puromycin-resistant gene [40] was used for the forced expression of the following cDNAs: mouse *Foxo1* (GenBank accession NM_019739.3: 466-2424) and human *PPP1R14C* (GenBank accession NM_030949.3: 150-647), and the catalytically inactive mutants of human *PP1α*, *PP1β/δ* and *PP1γ*, which have a single amino acid substitution in their catalytic domains (gifts from Dr. Y. Ikeda [41]). Expression vectors were transfected into ESCs using Xfect mESC Transfection Reagent (Clontech, Palo Alto, USA). After 1 or 2 days of transfection, cells were treated with 0.4 μg/ml puromycin and continuously cultured for more than one week. Puromycin-resistant cells were used for the induction of ESC differentiation. FOXO1 with reduced DNA binding activity [FOXO1 (HR)] [42] was generated by single amino acid substitution from histidine 212 in mouse FOXO1 to arginine by KOD FX (Toyobo, Osaka, Japan) using the following partially overlapping primers (lowercase letters represent the mutation): *Foxo1*(HR), fwd 5′-ATTCGCCgCAATCTGTCCCTTCACAG-3′ and rev 5′-CAGATTGcGGCGAATTGAATTCTTCC-3'.

Formation of EC colonies on the OP9 cell layer

VE-cadherin^{+} CD31^{+} ECs derived from F10-EGFP ESCs or EGFP-F/*Foxo1*$^{-/-}$ ESCs were FACS-purified and seeded on OP9 cell layers pre-formed in glass-bottomed dishes. Cells were cultured in induction medium supplemented with 10 ng/ml recombinant mouse VEGF-A165 (450-32, PeproTech, Rocky Hill, NJ, USA). After 4 or 5 days of culture, confocal images of living cells were acquired using an FV1000D confocal laser scanning microscope (Olympus, Tokyo, Japan). Contrast and brightness were equally adjusted over the original images using ImageJ software version 1.53q (National Institutes of Health, Bethesda, MD, USA). The shape of EC

colonies was classified into two types, i.e., sheet-like and cord-like. The sheet-like colony is a flat flagstone-like structure composed of polygonal-shaped ECs. The cord-like colony is a vessel-like structure composed of thin elongated ECs. The two types of EC colonies were manually counted under a fluorescent microscope and presented as a percentage of total EC colonies.

Formation of vessel-like structures in 3D spheroid culture

The formation of vessel-like structures in 3D spheroid culture was performed as previously reported [16] [18] [20]. In brief, ESC-derived $Flk1^+$ mesodermal cells were FACS-purified and aggregated. Cell aggregates were embedded in a type I collagen gel (Nitta Gelatin, Osaka, Japan) and cultured on a plastic disc (Cell Desk L, Sumitomo Bakelite) in induction medium containing 10 ng/ml VEGF-A165. After 4 or 5 days of culture, collagen gels were flattened by removing medium using filter paper and subjected to immunofluorescence staining [17] [18]. Confocal images were acquired using an FV1000D confocal laser scanning microscope. Contrast and brightness were equally adjusted over the original images using ImageJ software. The area of fluorescence staining was measured using ImageJ software. The extent of phosphorylated MLC2 (pMLC2) staining was assessed from the ratio of the total area of pMLC2 to the total area of actin, the ratio of the area of the merged region of pMLC2 and actin to the total area of actin, and the ratio of the total area of pMLC2 to the total area of ECs. The area of VE-$cadherin^+$ ECs was measured by manual tracing.

Targeted gene knockdown by siRNAs and co-transfection with plasmid DNA

The targeted knockdown of *FOXO1* or *PPP1R14C* genes was performed in HUVECs using siRNAs. *FOXO1* siRNA against the target sequence, 5'-CCGAAAACATGGAAAATCTTT-3', and *PPP1R14C* siRNA against the target sequence, 5'- ATGAAGAGAGAGCTTCAAAATTA-4', were designed using the siRNA online design site siDirect version 2.0 (http://sidirect2.rnai.jp/), and synthesized by Hokkaido System Science Co., Ltd. (Hokkaido, Japan). *FOXO1*- and *PPP1R14C*-specific siRNAs or Silencer Select Negative Control No. 1 siRNA (4390843, Thermo Fisher Scientific, Inc) were transfected into HUVECs using Lipofectamine RNAiMAX (13778100, Invitrogen, Carlsbad, CA, USA). The co-transfection of *FOXO1* siRNA and pCAGIPuro-human *PPP1R14C* into HUVECs was performed using ScreenFect A plus (293-77101, Wako). Cells 1–2 days after transfection were subjected to real-time PCR or a Western blot analysis.

Western blotting

Western blotting was performed as previously reported [20]. An anti-FOXO1 rabbit mAb (C29H4) (2880, Cell Signaling, 1:2000), anti-PPP1R14C (C-term) rabbit pAb (AP53404PU-N, Acris Antibodies GmbH, 1:500), anti-pMLC2 (Ser19) mouse mAb (3675, Cell Signaling, 1:1000), anti-MLC2 rabbit pAb (3672, Cell Signaling, 1:1000), and anti-b-actin rabbit pAb (20536-1-AP, ProteinTech, 1:2000) were used as primary antibodies. A horseradish peroxidase (HRP)-conjugated donkey anti-rabbit IgG antibody (NA934, Amersham, Buckinghamshire, UK) and HRP-conjugated horse anti-mouse IgG antibody (7076, Cell Signaling) were used as secondary antibodies.

3D sandwich culture for the formation of vascular cord structures

A 3D sandwich culture was performed as previously reported [20]. HUVECs were seeded on the bottom layer of a type I collagen gel (Collagen gel culture kit, Nitta Gelatin) and transfected with siRNA and the plasmid. Four

hours after transfection, cells were sandwiched with an upper layer of the collagen gel and cultured in the Endothelial Cell Growth Medium Kit (Takara) containing VEGF-A165 (10 ng/ml). After 2 days of culture, live cells were stained using green-fluorescent calcein-AM (06735-81, Nacalai Tesque, Kyoto, Japan). Images of the vascular cord structure were captured using an IX71 fluorescence microscope (Olympus). Contrast or brightness adjustments to define cord structures were applied equally over the original images using ImageJ software. A morphometric analysis of vascular cord structures was automatically analyzed in binary images converted from original images using ImageJ with the Angiogenesis Analyzer plugin tool [43]. “Cords” mentioned in the text include “isolated elements”, “branches”, and “segments” in the tool. “The average cord length” was calculated based on the value of “the total length of cords”/ “the number of cords” in each field.

Luciferase reporter assay

The upstream and intron sequences of the mouse and human *PPP1R14C* genes were amplified from mouse and human genomic DNA by PCR. The following primers were used (In-Fusion cloning sites are indicated by lowercase letters): the *Ppp1r14c* promoter fwd 5′-tggcctaactggccg TGTCCAACGTTTCAGAGCA-3′ and rev 5′-aggccagatcttgatc TAGGAAGTCGTCCGAGG-3′; enhancer (E)1 fwd 5′-tggcctaactggccg TTAGAGAGCATGGGGCTG-3′ and rev 5'-tcttgatatcctcga TGACGGAGCTCAGAACTC-3′; E2 fwd 5′-tggcctaactggccg CTCATGATCTTCTGTTTGCTAATCCTTCTT-3′ and rev 5′-tcttgatatcctcga ATAAGAATTAGTTGTGGGCATCAGCAGTAT-3′; E3 fwd 5′-tggcctaactggccg TCAAAGCATTTGCCAGAGTG-3′ and rev 5′-tcttgatatcctcga CAGTGCCCTCTTCTGTCCTC-3′; E2-1 fwd 5′-tggcctaactggccg AGAGGCCAAGGTTCAGAGTG-3′ and rev 5′-tcttgatatcctcga ATCTGCTGCCATCCCTTCTC-3′; E2-2 fwd 5′-tggcctaactggccg ACTCAACCAAGTGCCACAAA-3′ and rev 5′-tcttgatatcctcga CACTGCTTGCATAGTCTCAGG-3′; E2-2-1 fwd 5′-tggcctaactggccg ACTCAACCAAGTGCCACAAA-3′ and rev 5′-tcttgatatcctcga GTCCGCGGTTGGTGATAAAG-3′; E2-2-2 fwd 5′-tggcctaactggccg ACAGCAAGAGACCCAACCTT-3′ and rev 5′-tcttgatatcctcga CACTGCTTGCATAGTCTCAGG-3′; human enhancer (hE) fwd 5′-tggcctaactggccg TCCCATTTGACCCACATAAA-3′ and rev 5'-tcttgatatcctcga GACGGGGTCTTACCATGTTG-3′.

Mutations of the two putative FOXO1 binding sites in the E2-2-1 and hE region were generated by site-directed mutagenesis by KOD FX (Toyobo) using the following partially overlapping primers (the mutations are lowercased): MU1, fwd 5′-CGAGAtAGCtAAATTCGTAAAGTCTCTG-3′ and rev 5′-AATTTaGCTaTCTCGTTTTAAAAATGGG-3′; MU2, fwd 5′-GGATTCaGaTATTTCTTAGATGAACCAT-3′ and rev 5′-AGAAATAtCtGAATCCCATCAATAGTTC-3′; hMU1, fwd 5′-ATGAGAtAtCGGGGAGGCTCCAAGAGTCT-3′ and rev 5′-TCCCCGaTaTCTCATTTTAAAATGGAG-3′; hMu2, fwd 5′-GGATTCaGaTATTTCTCAAGTGAACCAT-3′ and rev 5′-AGAAATAtCtGAATCCTGTAAACTGTTC-3′.

PCR products were fused into the firefly luciferase reporter vector pGL4.27 (E8451, Promega, Madison, WI, USA) or pGL4.21 (E6761, Promega) using the In-Fusion HD Cloning Kit (Z9648N, Takara). Two complementary oligonucleotides containing three copies of the insulin response element (3×IRE) were cloned into the multi-cloning site of pGL4.27 [44]. The oligonucleotide sequences used were 5'-

tcgagCAAGCAAAACAAGCTAGCAAAACAAGTACGCAAAACAAGTa-3' and 5'-agcttACTTGTTTTGCGTACTTGTTTTGCTAGCTTGTTTTGCTTGc-3' (IRE are underlined and restriction sites are in lowercase).

UV2 cells or HUVECs were co-transfected with pRL-SV40 (E2231, Promega) and luciferase reporter vectors using Xfect mESC Transfection Reagent (Clontech). Luciferase activity was measured using the Dual Luciferase Reporter Assay System (E1910, Promega) and Mini Lumat LB 9506 (Berthold Technologies, Bad Wildbad, Germany).

CUT&RUN assay and quantitative real-time PCR

HUVECs were transfected with pCAGIPuro-mouse *Foxo1* using ScreenFect A plus (293-77101, Wako), and collected at 2 days. To analyze protein-DNA interactions, CUT&RUN assay kit (86652, Cell Signaling) was used according to the manufacturer's instructions. Each reaction used 250,000 living cells. An anti-FOXO1 rabbit mAb (C29H4) (2880, Cell Signaling, 1:50) and Rabbit (DA1E) mAb IgG XP Isotype Control (CUT&RUN) were used as a targeted antibody or a negative control antibody. DNA extracts were subjected to quantitative real-time PCR using THUNDERBIRD Next SYBR qPCR Mix (QPX-201, Toyobo) on the StepOne real-time PCR system (Applied Biosystems). The following primers were used: FOXO1 binding site-1 fwd 5'-TCCCATTTGACCCACATAAA-3' and rev 5'-CCTCCCCGTTTTCTCATTTT-3'; FOXO1 binding site-2 fwd 5'-CATTTTCAAATATGCTTCATCTTAGT-3' and rev 5'-CCTGTAAATGGTTCACTTGAGAAA-3'; alpha satellite repeat (SAT) fwd 5'-ACAGAGCGGATTGGAAACAC-3' and rev 5'-GGCCTCAAGGCTCTTGAAAT-3'. The signal of the target was normalized to the signal of sample normalization spike-in DNA (CUT&RUN) added into each reaction.

Isolation of ECs from mouse embryos

ECs were FACS-purified from embryonic day (E) 10.5 ICR mouse embryos as previously reported [20] and then subjected to the gene expression analyses described above.

Whole-mount immunostaining of forelimb vessels of mouse embryos

ECs in the forelimb vessels of E11.5 ICR mouse embryos were examined for the presence of pMLC2 using whole-mount immunostaining as previously reported [45]. The forelimb vessels of this stage are not yet surrounded by smooth muscle cells [46]. Fluorescence images were acquired using a FV1000D confocal laser scanning microscope. To examine the *in vivo* effects of the inhibition of MLCK, pregnant ICR mice were intraperitoneally injected with ML7 (13.58 mg/kg body weight) or DMSO, which were diluted in a mixture of propylene glycol, Tween 80, and 5% glucose (30:5:65), once daily for 3 days from E8.5 to E10.5. Embryos were collected at E11.5 and subjected to whole-mount immunostaining.

Microinjection into zebrafish embryos

A microinjection of antisense morpholino oligonucleotides (MO) into zebrafish embryos was performed to knockdown the expression of *foxo1a*, *foxo1b*, and *ppp1r14c*. The following splice-blocking MO were designed and synthesized by Gene Tools, LLC (Philomath, OR, USA): *foxo1a* MO 5'-

GTTTGGTAAGCAGCTTGTACCTTTT-3'; *foxo1b* MO 5'-TTGTTCTCCCCTCAACTGACCTTTT-3'; *ppp1r14c* MO 5'-GACAAAAACTGCACATTTACCTGCA-3'. Standard Control Oligo Classic (Gene Tools) (5'-CCTCTTACCTCAGTTACAATTTATA-3') was used as the MO control. MO was diluted to the indicated concentration in sterile water containing 0.05% phenol red (Wako) as a visible marker. The microinjection was performed using an SMZ745 stereoscopic microscope (Nikon, Tokyo, Japan) equipped with a FemtoJet 4i electronic microinjector (Eppendorf, Hamburg, Germany) and MM-3 micromanipulator (Narishige, Tokyo, Japan). Microinjection needles were made from glass capillaries with filament GD-1 (Narishige) using a PE-2 glass microelectrode puller (Narishige). The injection into the yolk of zebrafish embryos was performed at the 1–2 cell stage. The needle opening size was compensated for by the injection pressure condition and, as a result, was adjusted to the appropriate injection level.

Capped RNA was transcribed *in vitro* from the full-length mouse *Foxo1* gene (NM_019739.3) or full-length human *PPP1R14C* gene (NM_030949.3)M using the mMESSAGE mMACHINE SP6 Transcription kit (AM1340, Thermo Fisher Scientific), and then purified using QIAzol Lysis Reagent (Qiagen). A co-injection of wild-type mouse *Foxo1* mRNA with foxo1a/*b* MO or wild-type human *PPP1R14C* mRNA with ppp1r14c MO was performed for rescue experiments.

Following the microinjection, embryos were incubated at 28°C in E3 solution and allowed to develop until the indicated days post-fertilization (dpf). Embryos were anesthetized with tricaine and observed using an IX71 (Olympus) or Axio Imager 2 (Zeiss, Oberkochen, Germany) microscope. Fluorescence images were acquired using a FV1000 confocal microscope (Olympus). Body images were acquired using a Nikon ECLIPSE TS100 inverted microscope and Nikon DS-Fi3 Digital Camera (Nikon).

Analysis of the *in vivo* vascular structure

Fluorescence images of the vascular structure were converted to 8-bit images, and contrast and brightness adjustments were applied equally to the original images using ImageJ software. The vessel diameters of the mouse embryonic forelimb vasculature and the lengths of the intersegmental vessels (ISVs) of zebrafish embryos were measured by manual tracing using ImageJ software. The number of ISVs in an anterior part of the middle trunk region was counted.

Statistical analysis

The *F*-test followed by an unpaired, two-tailed *t* test was used to compare the two samples. Dunnett's or Tukey's multiple comparison test was performed using the MEPHAS web tool (http://www.gen-info.osaka-u.ac.jp/testdocs/tomocom/dunnett-e.html or http://www.gen-info.osaka-u.ac.jp/testdocs/tomocom/tukey-e.html, respectively) for multiple comparisons. Data are presented as the mean ± s.d. unless otherwise indicated. A P value <0.05 was considered to be significant.

Results

Gene expression profiling identifies FOXO1-dependent EC elongation-related genes

To identify candidate FOXO1 target genes that regulate EC elongation, we analyzed our previous DNA microarray dataset (NCBI GEO accession No. GSE76366) on the gene expression profiles of mouse ESC-ECs [19]. The dataset includes ECs derived from ESCs with two different genotypes (*Foxo1*$^{+/+}$ and *Foxo1*$^{-/-}$), both of which were cultured either in the presence or absence of a VEGF stimulation, and, thus, were categorized into four groups in Supplementary Fig. 1a. ECs in three groups, i.e., [*Foxo1*(-/-), VEGF(-)], [*Foxo1*(+/+), VEGF(-)], and [*Foxo1*(-/-), VEGF(+)], presented a flagstone-like morphology and formed sheet-like colonies. In contrast, ECs in the [*Foxo1*(+/+), VEGF(+)] group presented an elongated shape and formed cord-like colonies [47] [19] (Supplementary Fig. 1a).

To extract the genes specific for EC elongation, data from each of the three groups of flagstone-like ECs were separately compared to data from the group of elongated ECs [*Foxo1*(+/+), VEGF(+)]. Genes with expression levels that were lower in each of the flagstone-like EC groups than in the elongated EC group partially overlapped (Supplementary Fig. 1b). A total of 226 genes were commonly detected in all comparisons and designated EC elongation-related genes (ERGs) (Supplementary Fig. 1b, Supplementary Table 1). Consistent with the known functions of FOXO1, a gene ontology (GO) enrichment analysis of ERGs indicated terms such as metabolism and homeostatic process (Supplementary Table 2).

Comparison of two flagstone-like EC groups in a steady state without VEGF, [*Foxo1*(-/-), VEGF(-)] vs. [*Foxo1*(+/+), VEGF(-)] showed the 252 genes reduced in *Foxo1*$^{-/-}$ ECs (Supplementary Fig. 1c and Supplementary Table 3). Notably, most of these genes were not included in ERGs, and their GO terms were not shown in GO terms of ERGs (Supplementary Table 1-4). This result suggests that ERGs were more specifically associated with EC elongation among Foxo1-dependent genes.

PPP1R14C rescues the aberrant shape of *Foxo1*$^{-/-}$ ECs

After a pilot functional screening of several candidate genes extracted as ERGs by forced expression in *Foxo1*$^{-/-}$ ESC-ECs, we focused on the *Ppp1r14c* gene. Myosin activity influences cell morphology and is oppositely regulated by the phosphorylation and dephosphorylation of MLC2 induced by MLCK and MLC phosphatase (MLCP), respectively. MLCP is a holoenzyme consisting of three components, i.e., a catalytic subunit serine/threonine protein phosphatase 1 (PP1), a regulatory subunit myosin phosphatase target subunit 1 (MYPT1), and a small accessory subunit of 20/21 kDa (M20/21). The dephosphorylation of phosphorylated MLC2 (pMLC2) by MLCP relaxes the cytoskeletal tension. The PP1 activity of MLCP is inhibited by endogenous PP1 inhibitors, the PPP1R14 family proteins (for reviews, see [48] [49] [50]). PPP1R14C belongs to the PPP1R14 family and, thus, may be involved in the Foxo1-dependent regulation of EC morphology.

We initially confirmed in real-time PCR analyses that *Ppp1r14c* expression was significantly lower in *Foxo1*$^{-/-}$ ESC-ECs than in *Foxo1*$^{+/+}$ ESC-ECs, both of which were cultured in the presence of VEGF (Fig. 1a and b).

We then investigated whether the forced expression of PPP1R14C rescued the abnormal phenotype of *Foxo1*$^{-/-}$ ESC-ECs. EGFP-tagged ESC-ECs (wild-type ECs and *Foxo1*$^{-/-}$ ECs derived from F10-EGFP ESCs and EGFP-

F/*Foxo1*$^{-/-}$ ESCs, respectively) were sorted and allowed to form EC colonies on an OP9 cell layer in the presence of VEGF. Wild-type ESC-ECs were elongated and formed cord-like colonies (Fig. 1c and d, Supplementary Fig. 1a). In contrast, *Foxo1*$^{-/-}$ ESC-ECs failed to elongate and formed sheet-like colonies (Fig. 1c and d, Control; Supplementary Fig. 1a). The defect was rescued by the forced expression of the mouse *Foxo1* gene or human *PPP1R14C* gene, and colonies were restored to the normal cord-like morphology (Fig. 1c and d, FOXO1, PPP1R14C).

These results suggest that PPP1R14C contributes to EC elongation and the formation of cord-like colonies downstream of FOXO1.

Foxo1$^{-/-}$ ECs fail to phosphorylate MLC2

To examine whether decreased PPP1R14C expression resulted in the excessive dephosphorylation of pMLC2 in *Foxo1*$^{-/-}$ ECs, we compared the distribution of pMLC2 in *Foxo1*$^{+/+}$ and *Foxo1*$^{-/-}$ ECs. ESC-derived Flk1^{+} mesodermal cells (ESC-MCs) were sorted, aggregated, and cultured in a type I collagen gel containing VEGF to induce the formation of vessel-like structures (3D spheroid culture).

VE-cadherin-expressing ECs spread out from *Foxo1*$^{+/+}$ ESC-MC aggregates and formed thin and long vessel-like structures. pMLC2 colocalized with actin filaments along the cell circumference (Fig. 1e and f). In contrast, *Foxo1*$^{-/-}$ ECs formed abnormal thick and short bundles with a disordered distribution of actin filaments instead of thin and long vessel structures (Fig. 1e and f). pMLC2 was not detected in aberrant EC bundles, albeit cells proximal to the body of aggregates had a low level of pMLC2. The total and actin-merged area of pMLC2 staining was significantly lower in *Foxo1*$^{-/-}$ ECs than in *Foxo1*$^{+/+}$ ECs (Fig. 1g–i).

This result suggests that the phosphorylation of MLC2 was severely attenuated in *Foxo1*$^{-/-}$ ECs.

PP1 inhibition recovers MLC2 phosphorylation and rescues the abnormal morphology of _Foxo1_$^{-/-}$ ECs

We investigated whether the inhibition of PP1 phosphatase activity reversed the phenotype of *Foxo1*$^{-/-}$ ESC-ECs. We introduced dominant-negative (dn) forms of the human PP1 isoforms, dn PP1 α, dn PP1β/δ, and dn PP1γ into EGFP-F/*Foxo1*$^{-/-}$ ESCs. All dn PP1 isoforms increased the ratio of cord-like colonies, albeit to a lesser extent than the forced expression of FOXO1 (Fig. 2a and b).

In the 3D spheroid culture of *Foxo1*$^{-/-}$ ESC-MCs, the induction of FOXO1, PPP1R14C, or dn PP1α, converted aberrant EC bundles to thin vessel-like structures (Fig. 2c). Phenotypically rescued *Foxo1*$^{-/-}$ ECs markedly increased pMLC2 level, which co-localized with actin filaments (Fig. 2c–f). Consistent with this result, PP1 inhibition by a chemical inhibitor, tautomycetin, also recovered the distribution of pMLC2 and actin filaments in *Foxo1*$^{-/-}$ ECs and induced the formation of vessel-like structures (Supplementary Fig. 2). Tautomycetin did not affect in *Foxo1*$^{+/+}$ ECs. In contrast, MLCK inhibition by a chemical inhibitor, ML7, induced the loss of MLC2 phosphorylation and an irregular cell morphology with a disordered distribution of actin filaments in *Foxo1*$^{+/+}$ ECs (Supplementary Fig. 2). *Foxo1*$^{-/-}$ EC bundles remained nearly unchanged in the presence of ML7 from those in the untreated groups.

These results suggest that FOXO1-dependent EC elongation requires MLC2 phosphorylation by the inhibition of PP1 activity, which PPP1R14C exerts under physiological conditions.

FOXO1-knockdown reduces PPP1R14C expression and MLC2 phosphorylation in HUVECs, thereby suppressing cord formation

The ESC-EC differentiation system provided an important clue on the mechanisms of EC elongation during angiogenesis. Next, HUVECs were used to validate these observations in a system relevant to human vascular tissue and exclude uncommon phenomena in a specific ES cell line. The siRNA-mediated knockdown of *FOXO1* in HUVECs (Fig. 3a, c, and d) was performed to evaluate the role of FOXO1 in human ECs. *FOXO1*-knockdown reduced *PPP1R14C* expression at the mRNA and protein levels (Fig. 3b, c, and e). MLC2 phosphorylation also significantly decreased (Fig. 3c and f). In type I collagen gel sandwich cultures of HUVECs, *FOXO1*-knockdown decreased the number and length of vascular cords (Fig. 3g–j). These effects of *FOXO1*-knockdown in HUVECs are essentially in line with the findings of *Foxo1*$^{-/-}$ ESC-ECs (Fig. 1a and b). However, *FOXO1*-knockdown did not cause the dilation of vascular cords, similar to results of the previous report [3]. To confirm the involvement of PPP1R14C in FOXO1-regulated angiogenesis, HUVECs were simultaneously transfected with *FOXO1* siRNA and *PPP1R14C* expression vectors (Fig. 3k and l). The forced expression of PPP1R14C rescued cord formation that was inhibited by *FOXO1*-knockdown (Fig. 3m–p). Consistent with this result, *PPP1R14C*-knockdown in HUVECs reduced MLC2 phosphorylation and inhibited cord formation (Supplementary Fig. 3).

These results suggest that FOXO1 regulates vascular cord formation by HUVECs through PPP1R14C expression and MLC2 phosphorylation.

The chemical inhibition of PP1 by tautomycetin recovered the cord formation inhibited by *FOXO1*- or *PPP1R14C*-knockdown (Supplementary Fig. 4). Okadaic acid, a PP1 and PP2A inhibitor that requires higher concentrations to inhibit PP1 than PP2A, failed to reverse the suppressed cord formation in *FOXO1*- or *PPP1R14C*-knockdown.

FOXO1 activates the enhancer element located in the first intron of the _PPP1R14C_ gene

We investigated whether FOXO1 directly regulated *PPP1R14C* gene transcription. Luciferase reporter analyses were performed using the mouse EC line, UV2 cells (Supplementary Fig. 5), and HUVECs (Fig. 4). FOXO1 binds to recognition elements, such as insulin response element (IRE), which contains the consensus sequence 5'-TT(G/A)TTTTG-3' [44]. The transcriptional activity of induced FOXO1 was confirmed by the activation of three copies of IRE (3×IRE) (Supplementary Fig. 5d).

Reporter activity of a genomic region encompassing the promoter of the mouse *Ppp1r14c* gene (p*Ppp1r14c*) was elevated regardless of the induction of FOXO1 in UV2 cells, suggesting that the activity of the *Ppp1r14c* promoter was independent of FOXO1 (Supplementary Fig. 5a, b, and d). We then evaluated three genomic regions located upstream (E1), intron 1 (E2), and intron 4 (E3), which were rich in putative FOXO1 binding sites conserved between mice and humans (Supplementary Fig. 5a and b). Among the three regions, only E2 showed significantly

higher activity in the presence of FOXO1 (Supplementary Fig. 5e). Analyses of two subregions of E2 (E2-1 and E2-2) demonstrated the E2-2 enhancer activity increased by FOXO1 (Supplementary Fig. 5f). E2-2 was not activated by a DNA-binding-defective FOXO1 mutant [FOXO1 (HR)] (Supplementary Fig. 5g), suggesting a dependence on the direct binding of FOXO1.

We analyzed two overlapping subregions of E2-2 (E2-2-1 and E2-2-2) and detected enhancer activity in E2-2-1, which was enhanced by FOXO1, but not by FOXO1 (HR) (Supplementary Fig. 5h). Two putative FOXO1 binding sites were present in E2-2-1 (Supplementary Fig. 5c). Mutations disrupting the binding motifs at either site did not affect enhancer activity, while mutations in both sites significantly reduced activity (Supplementary Fig. 5i). These results revealed a FOXO1-regulated enhancer element in the first intron of the mouse *Ppp1r14c* gene.

The first intron of the human *PPP1R14C* gene had a putative enhancer region (hE) similar to the identified mouse *Ppp1r14c* enhancer, E2-2-1 (Fig. 4a and b). hE contained two putative binding sites of FOXO1. A reporter analysis using HUVECs showed the significantly higher activity of hE in the presence of FOXO1 (Fig. 4c). Similar to the mouse *Ppp1r14c* enhancer activity, hE activity was abolished by mutations in the binding motifs of both FOXO1 binding sites (Fig. 4c).

We performed a CUT&RUN assay on HUVECs with an anti-FOXO1 antibody to analyze the DNA-protein interaction. Real-time PCR analyses of the CUT&RUN products showed the relative enrichment of FOXO1 on the FOXO1 binding site-1 and FOXO1 binding site-2 of hE (Fig. 4d).

These results suggest that the transcription of the *PPP1R14C* gene is positively and directly regulated by FOXO1 through two binding sites in an enhancer element that is conserved in mice and humans.

MLCK inhibition causes an abnormal vascular structure in mouse embryos

To detect the mRNA expression of *Foxo1* and essential genes regulating MLC2 phosphorylation in developing ECs, an RT-PCR analysis of $CD45^{-}$ $CD31^{+}$ VE-$cadherin^{+}$ $Flk1^{+}$ ECs isolated from whole mouse embryos at embryonic day (E) 10.5 was performed. These transcripts were detected in embryonic ECs (Fig. 5a) and two EC lines, UV2 cells and bEnd.3 cells (Fig. 5a). bEnd.3 cells showed the reduced expression of *Ppp1r14c*. While cultured ECs usually take a polygonal or epithelial-like morphology, bEnd.3 cells have an elongated fibroblastic-like shape [51][52][20], which may reflect the difference in *Ppp1r14c* expression.

Whole-mount immunostaining of E11.5 mouse embryos revealed the presence of pMLC2 in ECs, which were identified in the forelimb vessels by VE-cadherin, IB4, and Flk1 staining (Fig. 5b and c). To examine the role of pMLC2 in angiogenesis in mouse embryos, ML7 was intraperitoneally administered to pregnant mice once a day for 3 days from E8.5. Type IV collagen immunostaining showed that MLCK inhibition induced abnormalities in E11.5 forelimb vessels; vessels were thicker and more dilated than those in the control (Fig. 5d). Vessel diameters were significantly larger in the proximal and distal regions of the treated forelimbs (Fig. 5e and f).

These results suggest that ECs in developing vessels express *Foxo1* and *Ppp1r14c* and maintain phosphorylated MLC2, which is required for normal vascular development during embryogenesis.

foxo1-knockdown causes an abnormal vascular structure in zebrafish embryos

Zebrafish ECs express orthologs of the mammalian *FOXO1* gene, namely, *foxo1a* and *foxo1b* (NCBI GEO accession No. GSE119718). RT-PCR analyses confirmed the expression of these genes in zebrafish embryos (Fig. 6a). We knocked down the *foxo1a* and *foxo1b* genes by injecting antisense morpholino oligonucleotide (MO) into *Tg(fli1a:Myr-mCherry)* transgenic embryos (Fig. 6b).

The *foxo1a/b*-simultaneous knockdown decreased the length of the intersegmental vessels (ISVs) (Fig. 6c–e). ISVs in the *foxo1a*/*b* morphants exhibited disturbances at the edges and failed to connect with the dorsal longitudinal anastomotic vessel (DLAV) (Fig. 6c, d, and f). Moreover, the caudal vein plexus (CVP) in the *foxo1a*/*b* morphants lacked a space segregating the dorsal vein (DV) and ventral vein (VV) [53] (Fig. 6c, d, and g). Single morphants of *foxo1a* or *foxo1b* also showed similar, but less severe, phenotypes (Supplementary Fig. 6). Abnormalities in the *foxo1a*/*b* morphants were mostly rescued by exogenously expressed mouse *Foxo1* (Supplementary Fig. 7a and Fig. 6d–g).

These results suggest that an overlapping function of the *foxo1a* and *foxo1b* genes are essential for normal vascular development in zebrafish embryos. The *foxo1a/b* morphants showed highly observable body curvature. However, the defect was recovered by the forced expression of *Foxo1* (Supplementary Fig. 8a and b), implying the importance of *foxo1* in the normal development of zebrafish.

PPP1R14C regulates the vascular structure in zebrafish embryos downstream of FOXO1

RT-PCR analyses detected the expression of essential genes regulating MLC2 phosphorylation in zebrafish embryos (Fig. 7a). We investigated whether *ppp1r14c*-knockdown (Fig. 7b) resulted in the same phenotype observed in the vasculature of the *foxo1a*/*b* morphants. *ppp1r14c*-knockdown decreased the ISV length and induced malformations in DLAV and CVP, similar to *foxo1a*/*b*-knockdown (Fig. 7c–f). These abnormalities were rescued by the exogenous expression of human *PPP1R14C* (Supplementary Fig. 7b and Fig. 7c–f). The *ppp1r14c* morphants also exhibited body curvature but with moderate frequency (Supplementary Fig. 8c and d).

We next examined whether *ppp1r14c* was located downstream of *foxo1a* and *foxo1b* in the regulation of the vascular structure in zebrafish embryos. *foxo1a/b*-simultaneous knockdown reduced the *ppp1r14c* expression, suggesting the dependency of *ppp1r14c* expression on *foxo1* (Fig. 8a). The exogenous expression of human PPP1R14C recovered the decreased ISV length in the *foxo1a*/*b* morphants (Fig. 8b and c). PPP1R14C-induction also attenuated structural abnormalities in DLAV and CVP in the *foxo1a*/*b* morphants (Fig. 8b, d, and e).

These results suggest that the abnormal vascular structure caused by *foxo1*-knockdown in zebrafish embryos is largely due to the decreased expression of the *ppp1r14c* gene.

Consistent with the results of HUVECs (Supplementary Fig. 4), the inhibition of PP1 by tautomycetin restored

vascular abnormalities in *foxo1a*/b or *ppp1r14c* morphants (Supplementary Fig. 9), suggesting that PP1 activity is involved in EC elongation regulated by *foxo1* through *ppp1r14c* transcription.

Discussion

The present study investigated the downstream mechanism of FOXO1-dependent EC elongation. We identified the *Ppp1r14c* gene as a candidate for FOXO1 target genes that are closely associated with EC elongation. Notably, most ERGs, including *Ppp1r14c*, were not extracted by comparing wild-type ECs and *Foxo1*$^{-/-}$ ECs in a steady state, i.e., without a VEGF stimulation. Therefore, the gene expression landscape is suggested to dynamically change in EC elongation. *Ppp1r14c* expression was decreased in *Foxo1*$^{-/-}$ ESC-ECs, and the forced expression of PPP1R14C rescued *Foxo1*$^{-/-}$ ESC-ECs from a deficiency in cell elongation. *FOXO1*-knockdown in HUVECs reduced *PPP1R14C* expression and suppressed vascular cord formation, which was restored by the forced expression of PPP1R14C. We identified a novel FOXO1-responsive enhancer element conserved in the human and mouse *Ppp1r14c* gene locus. The element contains two putative FOXO1 binding sites, which are less homologous to the typical consensus sequence. A mutant FOXO1 deficient for DNA binding did not activate the enhancer element, and FOXO1 directly interacted with the element. Despite the known inhibitory effects of FOXO1 in EC growth and metabolism, our study suggests that FOXO1 may also have a supportive role in angiogenesis.

The phosphorylation status of MLC2 in ECs has been associated with angiogenesis in several studies. A co-culture system of HUVECs and human dermal fibroblasts showed that MLC2 phosphorylation was suppressed during the migratory phase of ECs and subsequently increased after the establishment of long tubes [28] [29]. MLCK inhibition by ML7 attenuated vessel formation by HUVECs in a 3D fibrin gel culture [54]. Conversely, the inhibition of PP1 and PP2A by okadaic acid (5-50000 fmol/egg) induced angiogenesis on the chorioallantoic membrane of chick embryos [55]. Okadaic acid (10 or 100 nmol/L) also promoted the formation of a capillary network by HUVEC-matrigel culture [56]. Our present study found that MLC2 phosphorylation was suppressed in *Foxo1*$^{-/-}$ ESC-ECs, possibly due to the loss of PPP1R14C. MLC2 phosphorylation was restored by inducing PPP1R14C concomitantly with recovery from a deficiency in cell elongation. PP1 inhibition by the introduction of dominant-negative forms or tautomycetin treatment also induced MLC2 phosphorylation and cell elongation by *Foxo1*$^{-/-}$ ESC-ECs. In contrast, MLCK inhibition by ML7 diminished MLC2 phosphorylation in wild-type ESC-ECs and impaired vessel-like structures, which resembled the phenotype of *Foxo1*$^{-/-}$ ESC-ECs. *FOXO1* or *PPP1R14C*-knockdown in HUVECs also suppressed MLC2 phosphorylation and vascular cord formation. The vascular defects caused by *FOXO1* or *PPP1R14C*-knockdown were reversed by tautomycetin but not by okadaic acid at the same concentration (1 nmol/L). As the concentration of okadaic acid was lower than that used in the previous report [56] and may not be sufficient to inhibit PP1 compared to PP2A, the result suggests the importance of PP1, rather than PP2, in FOXO1 and PPP1R14C-dependent EC elongation.

The present and previous findings suggest that MLC2 phosphorylation is required for EC elongation and normal vascular formation. Based on the results obtained herein, FOXO1 appears to play a role in the regulation of MLC2 phosphorylation via PPP1R14C.

The FOXO1-PPP1R14C-MLC2 axis is not an *in vitro* artificial phenomenon. The present study demonstrated that *foxo1*-knockdown in zebrafish embryos diminished *ppp1r14c* expression and caused vascular malformation in ISV, DLAV, and CVP. *ppp1r14c*-knockdown reproduced the same vascular phenotype as the *foxo1* morphants. The induction of PPP1R14C in *foxo1* morphants restored the vascular phenotype. PP1 inhibition by tautomycetin restored vascular defects in *foxo1a/b* or *ppp1r14c* morphants. ISVs were previously reported to be formed by sprouting angiogenesis, while CVP was formed by the coordination of sprouting and intussusceptive angiogenesis [57][53][58]. It currently remains unclear whether FOXO1 solely regulates sprouting angiogenesis or exerts its role in different types of angiogenesis. The growth of blood vessels results from a combination of different EC activities, including proliferation, migration, elongation, and motility. A computational model indicates the primary effect of proliferation rate on the extent of vessel growth [59]. However, in an analysis of the cell-cycle progression of zebrafish ECs, the formation of ISVs and caudal vessels has been reported not to require EC division necessarily [35]. Furthermore, different modes have been recognized for the elongation of tube structures, including cell proliferation and individual cell elongation without cell proliferation (for a review, see [60]). We demonstrated that FOXO1-disruption causes morphological defects during *in vitro* angiogenesis and *in vivo* vascular development. Taken together with our and other studies, the failure of the elongation function at the cellular level has a significant impact on the *in vivo* phenotypes of *foxo1* and *ppp1r14c* morphants. However, the contributions of multiple cellular activities in vascular development should be carefully considered.

In addition, we demonstrated the dilated forelimb vessels by the administration of ML7 in mouse embryos, suggesting that MLC2 phosphorylation is also required for vascular development in the mouse. Nevertheless, a rescue experiment using *Foxo1*$^{-/-}$ mouse embryos, e.g., PPP1R14C induction and PP1 inhibitor administration, has been hampered by the severe growth retardation and lethality of *Foxo1*$^{-/-}$ mouse embryos [7].

Another FOXO member, FOXO3, has also been reported to regulate EC functions such as migration and sprout formation [11]. In addition, Rho and Rho-associated coiled-coil containing protein kinase (ROCK) pathway regulates MLC2 phosphorylation, and chemical or genetic inhibition of ROCK suppresses vascular formation in *ex vivo* or *in vitro* angiogenesis models [61]. On the other hand, our gene expression profiles showed that FOXO3 and Rho-ROCK-related genes were not detected as ERGs, although some differences in the expression levels may be seen in some comparisons (Supplementary Table 1 and 5). This suggests that FOXO3 and Rho-ROCK are not principal targets of FOXO1 in EC elongation. However, the involvement of FOXO3 and Rho–ROCK pathway in FOXO1-dependent EC elongation cannot be entirely ruled out, as we previously reported [19][17], and further efforts are needed to elucidate the mechanisms that regulate EC elongation comprehensively.

Based on previous and present findings, we propose a novel model for the mechanism underlying FOXO1-regulated EC elongation (Supplementary Fig. 10). In this model, FOXO1 inhibits MLCP by up-regulating *PPP1R14C* gene expression in ECs, thereby promoting MLC2 phosphorylation and cell elongation during angiogenesis. Our findings appear to contradict the suppressive function of FOXO1 on EC activities by Potente et al.'s study [11]. FOXOs are a pleiotropic transcription factor; the cellular context determines the phenomena observed (for reviews, see [6] [14]). In cancer research, for instance, conflicting views of the role of FOXOs have

been reported; a negative regulator inhibiting growth and survival or a positive regulator promoting homeostasis, metastasis, and resistance to therapy (for a review, see [6]). FOXO1 function is highly dependent on the cellular environment, such as cell adhesion condition and growth factor levels, and the pleiotropic nature of FOXO1 may also influence angiogenic phenotypes of ECs, being reflected by the differences in the experimental conditions in each study.

Altered FOXO1 expression is associated with various pathological conditions. High expression of FOXO1 has been linked to hepatic insulin resistance in human [62], accelerated atherosclerosis in β-thalassemia major patients [63], and the survival prognosis in kidney or liver cancer patients (The Human Protein Atlas, https://www.proteinatlas.org). MLC2 phosphorylation correlates with an endothelial state in diseases, such as diabetes and tumorigenesis. Endothelial colony-forming cells from gestational diabetic pregnancies showed an increase in MLC2 phosphorylation [64]. Lovastatin, an HMG-CoA reductase inhibitor that suppresses tumor angiogenesis, reduced MLC2 phosphorylation in HUVECs [65] [66]. Therefore, our model may provide novel insights into the pathogenesis of disordered angiogenesis as well as the mechanisms regulating normal vascular development.

References

1. Accili D, Arden KC (2004) FoxOs at the crossroads of cellular metabolism, differentiation, and transformation. Cell 117:421–426. https://doi.org/10.1016/s0092-8674(04)00452-0.
2. Salih DA, Brunet A (2008) FoxO transcription factors in the maintenance of cellular homeostasis during aging. Curr Opin Cell Biol 20:126–136. https://doi.org/10.1016/j.ceb.2008.02.005
3. Kim YH, Choi J, Yang MJ, et al (2019) A MST1–FOXO1 cascade establishes endothelial tip cell polarity and facilitates sprouting angiogenesis. Nat Commun 10:. https://doi.org/10.1038/s41467-019-08773-2
4. Tsuchiya K, Tanaka J, Shuiqing Y, et al (2012) FoxOs integrate pleiotropic actions of insulin in vascular endothelium to protect mice from atherosclerosis. Cell Metab 15:372–381. https://doi.org/10.1016/j.cmet.2012.01.018
5. Benchoula K, Arya A, Parhar IS, Hwa WE (2021) FoxO1 signaling as a therapeutic target for type 2 diabetes and obesity. Eur J Pharmacol 891:. https://doi.org/10.1016/j.ejphar.2020.173758
6. Hornsveld M, Dansen TB, Derksen PW, Burgering BMT (2018) Re-evaluating the role of FOXOs in cancer. Semin Cancer Biol 50:90–100
7. Furuyama T, Kitayama K, Shimoda Y, et al (2004) Abnormal angiogenesis in Foxo1 (Fkhr)-deficient mice. Journal of Biological Chemistry 279:34741–34749. https://doi.org/10.1074/jbc.M314214200
8. Hosaka T, Biggs III WH, Tieu D, et al (2004) Disruption of forkhead transcription factor (FOXO) family members in mice reveals their functional diversification. Proc Natl Acad Sci U S A 101:2975–2980. https://doi.org/10.1073/pnas.0400093101
9. Sengupta A, Chakraborty S, Paik J, et al (2012) FoxO1 is required in endothelial but not myocardial cell lineages during cardiovascular development. Developmental Dynamics 241:803–813. https://doi.org/10.1002/dvdy.23759
10. Dharaneeswaran H, Abid MR, Yuan L, et al (2014) FOXO1-mediated activation of akt plays a critical role in vascular homeostasis. Circ Res 115:238–251. https://doi.org/10.1161/CIRCRESAHA.115.303227
11. Potente M, Urbich C, Sasaki KI, et al (2005) Involvement of Foxo transcription factors in angiogenesis and postnatal neovascularization. Journal of Clinical Investigation 115:2382–2392. https://doi.org/10.1172/JCI23126

12. Wilhelm K, Happel K, Eelen G, et al (2016) FOXO1 couples metabolic activity and growth state in the vascular endothelium. Nature 529:216–220. https://doi.org/10.1038/nature16498
13. Brent MM, Anand R, Marmorstein R (2008) Structural Basis for DNA Recognition by FoxO1 and Its Regulation by Posttranslational Modification. Structure 16:1407–1416. https://doi.org/10.1016/j.str.2008.06.013
14. Ren L, Yang J, Wang J, et al (2021) The roles of FOXO1 in periodontal homeostasis and disease. J Immunol Res 2021:. https://doi.org/10.1155/2021/5557095
15. Hirashima M, Kataoka H, Nishikawa S, et al (1999) Maturation of Embryonic Stem Cells Into Endothelial Cells in an In Vitro Model of Vasculogenesis. Blood 93:1253–1263
16. Yamashita J, Itoh H, Hirashima M, et al (2000) Flk1-positive cells derived from embryonic stem cells serve as vascular progenitors. Nature 408:92–96. https://doi.org/doi: 10.1038/35040568.
17. Matsukawa M, Sakamoto H, Kawasuji M, et al (2009) Different roles of Foxo1 and Foxo3 in the control of endothelial cell morphology. Genes to Cells 14:1167–1181. https://doi.org/10.1111/j.1365-2443.2009.01343.x
18. Park S-H, Sakamoto H, Tsuji-Tamura K, et al (2009) Foxo1 is essential for in vitro vascular formation from embryonic stem cells. Biochem Biophys Res Commun 390:. https://doi.org/10.1016/j.bbrc.2009.10.063
19. Tsuji-Tamura K, Ogawa M (2016) Inhibition of the PI3K-Akt and mTORC1 signaling pathways promotes the elongation of vascular endothelial cells. J Cell Sci 129:1165–1178. https://doi.org/10.1242/jcs.178434
20. Tsuji-Tamura K, Morino-Koga S, Suzuki S, Ogawa M (2021) The canonical smooth muscle cell marker TAGLN is present in endothelial cells and is involved in angiogenesis. J Cell Sci 134:. https://doi.org/10.1242/jcs.254920
21. Tsuji-Tamura K, Ogawa M (2018) Morphology regulation in vascular endothelial cells. Inflamm Regen 38:. https://doi.org/10.1186/s41232-018-0083-8
22. Levayer R, Lecuit T (2012) Biomechanical regulation of contractility: Spatial control and dynamics. Trends Cell Biol 22:61–81. https://doi.org/10.1016/j.tcb.2011.10.001
23. Vicente-Manzanares M, Ma X, Adelstein RS, Horwitz AR (2009) Non-muscle myosin II takes centre stage in cell adhesion and migration. Nat Rev Mol Cell Biol 10:778–790. https://doi.org/10.1038/nrm2786
24. Pearson RB, Jakes R, John M, et al (1984) Phosphorylation site sequence of smooth muscle myosin light chain (Mr = 20 000). FEBS Lett 168:108–112. https://doi.org/10.1016/0014-5793(84)80216-1
25. Sitbon YH, Yadav S, Kazmierczak K, Szczesna-Cordary D (2020) Insights into myosin regulatory and essential light chains: a focus on their roles in cardiac and skeletal muscle function, development and disease. J Muscle Res Cell Motil 41:313–327. https://doi.org/10.1007/s10974-019-09517-x
26. Molinar-Inglis O, Wozniak JM, Grimsey NJ, et al (2022) Phosphoproteomic analysis of thrombin- and p38 MAPK-regulated signaling networks in endothelial cells. Journal of Biological Chemistry 298:. https://doi.org/10.1016/j.jbc.2022.101801
27. Kunimura K, Miki S, Takashima M, Suzuki J ichiro (2021) S-1-propenylcysteine improves TNF-α-induced vascular endothelial barrier dysfunction by suppressing the GEF-H1/RhoA/Rac pathway. Cell Communication and Signaling 19:. https://doi.org/10.1186/s12964-020-00692-w
28. Mavria G, Vercoulen Y, Yeo M, et al (2006) ERK-MAPK signaling opposes Rho-kinase to promote endothelial cell survival and sprouting during angiogenesis. Cancer Cell 9:33–44. https://doi.org/10.1016/j.ccr.2005.12.021
29. Abraham S, Yeo M, Montero-Balaguer M, et al (2009) VE-Cadherin-Mediated Cell-Cell Interaction Suppresses Sprouting via Signaling to MLC2 Phosphorylation. Current Biology 19:668–674. https://doi.org/10.1016/j.cub.2009.02.057
30. Shen Q, Rigor RR, Pivetti CD, et al (2010) Myosin light chain kinase in microvascular endothelial barrier function. Cardiovasc Res 87:272–280. https://doi.org/10.1093/cvr/cvq144
31. Tsuji-Tamura K, Sato M, Fujita M, Tamura M (2020) The role of PI3K/Akt/mTOR signaling in dose-dependent biphasic effects of glycine on vascular development. Biochem Biophys Res Commun 529:596–602. https://doi.org/10.1016/j.bbrc.2020.06.085
32. Nakahara M, Tateyama H, Araki M, et al (2013) Gene-trap mutagenesis using Mol/MSM-1

embryonic stem cells from MSM/Ms mice. Mammalian Genome 24:228–239. https://doi.org/10.1007/s00335-013-9452-4
33. De Val S, Chi NC, Meadows SM, et al (2008) Combinatorial Regulation of Endothelial Gene Expression by Ets and Forkhead Transcription Factors. Cell 135:1053–1064. https://doi.org/10.1016/j.cell.2008.10.049
34. Kodama H, Niida S, Nishikawa S (1994) Involvement of the c-kit receptor in the adhesion of hematopoietic stem cells to stromal cells. Exp Hematol 22:979–984
35. Fukuhara S, Zhang J, Yuge S, et al (2014) Visualizing the cell-cycle progression of endothelial cells in zebrafish. Dev Biol 393:10–23. https://doi.org/10.1016/j.ydbio.2014.06.015
36. Avdesh A, Chen M, Martin-Iverson MT, et al (2012) Regular care and maintenance of a Zebrafish (Danio rerio) laboratory: An introduction. Journal of Visualized Experiments. https://doi.org/10.3791/4196
37. Nüsslein-Volhard C, Dahm R (2002) Zebrafish: A Practical Approach (The Practical Approach Series). Oxford University Press
38. Matsuyoshi N, Toda K, Horiguchi Y, et al (1997) In vivo evidence of the critical role of cadherin-5 in murine vascular integrity. Proc Assoc Am Physicians 109:362–71
39. Kataoka H, Takakura N, Nishikawa S, et al (1997) Expressions of PDGF receptor alpha, c-Kit and Flk1 genes clustering in mouse chromosome 5 define distinct subsets of nascent mesodermal cells. Dev Growth Differ 39:729–769
40. Niwa H, Yamamura K, Miyazaki J (1991) Efficient selection for high-expression transfectants with a novel eukaryotic vector. Gene 108:193–199. https://doi.org/10.1016/0378-1119(91)90434-d.
41. Aoyama H, Ikeda Y, Miyazaki Y, et al (2011) Isoform-specific roles of protein phosphatase 1 catalytic subunits in sarcoplasmic reticulum-mediated Ca2 cycling. Cardiovasc Res 89:79–88. https://doi.org/10.1093/cvr/cvq252
42. Tang ED, Nuñ Ez ¶ G, Barr FG, Guan K-L (1999) Negative regulation of the forkhead transcription factor FKHR by Akt. J Biol Chem 274:16741–16746. https://doi.org/10.1074/jbc.274.24.16741.
43. Carpentier G, Berndt S, Ferratge S, et al (2020) Angiogenesis Analyzer for ImageJ — A comparative morphometric analysis of "Endothelial Tube Formation Assay" and "Fibrin Bead Assay." Sci Rep 10:. https://doi.org/10.1038/s41598-020-67289-8
44. Guo S, Rena G, Cichy S, et al (1999) Phosphorylation of Serine 256 by Protein Kinase B Disrupts Transactivation by FKHR and Mediates Effects of Insulin on Insulin-like Growth Factor-binding Protein-1 Promoter Activity through a Conserved Insulin Response Sequence. J Biol Chem 274:17184–17192. https://doi.org/10.1074/jbc.274.24.17184.
45. Yokomizo T, Dzierzak E (2010) Three-dimensional cartography of hematopoietic clusters in the vasculature of whole mouse embryos. Development 137:3651–3661. https://doi.org/10.1242/dev.051094
46. Shoham A ben, Malkinson G, Krief S, et al (2012) S1P1 inhibits sprouting angiogenesis during vascular development. Development (Cambridge) 139:3859–3869. https://doi.org/10.1242/dev.078550
47. Furuyama T, Nakazawa T, Nakano I, Mori N (2000) Identification of the differential distribution patterns of mRNAs and consensus binding sequences for mouse DAF-16 homologues. Biochem J 349:629–634
48. Eto M (2009) Regulation of cellular protein phosphatase-1 (PP1) by phosphorylation of the CPI-17 family, C-kinase-activated PP1 Inhibitors. Journal of Biological Chemistry 284:35273–35277. https://doi.org/10.1074/jbc.R109.059972
49. Eto M, Brautigan DL (2012) Endogenous inhibitor proteins that connect Ser/Thr kinases and phosphatases in cell signaling. IUBMB Life 64:732–739
50. Matos B, Howl J, Jerónimo C, Fardilha M (2021) Modulation of serine/threonine-protein phosphatase 1 (PP1) complexes: A promising approach in cancer treatment. Drug Discov Today 26:2680–2698. https://doi.org/10.1016/j.drudis.2021.08.001
51. Tsuji-Tamura K, Ogawa M (2018) Dual inhibition of mTORC1 and mTORC2 perturbs cytoskeletal organization and impairs endothelial cell elongation. Biochem Biophys Res Commun 497:326–331. https://doi.org/10.1016/j.bbrc.2018.02.080

52. Tsuji-Tamura K, Tamura M (2022) Basic fibroblast growth factor uniquely stimulates quiescent vascular smooth muscle cells and induces proliferation and dedifferentiation. FEBS Lett 596:1686–1699. https://doi.org/10.1002/1873-3468.14345
53. Karthik S, Djukic T, Kim JD, et al (2018) Synergistic interaction of sprouting and intussusceptive angiogenesis during zebrafish caudal vein plexus development. Sci Rep 8:. https://doi.org/10.1038/s41598-018-27791-6
54. Kniazeva E, Putnam AJ (2009) Endothelial cell traction and ECM density influence both capillary morphogenesis and maintenance in 3-D. Am J Physiol Cell Physiol 297:179–187. https://doi.org/10.1152/ajpcell.00018.2009.-Identifying
55. Oikawa T, Suganuma M, Ashino-Fuse H, Shimamura M (1992) Okadaic acid is a potent angiogenesis inducer. Jpn J Cancer Res 83:6–9. https://doi.org/10.1111/j.1349-7006.1992.tb02343.x
56. Kim YS, Ahn KH, Kim SY, Jeong JW (2009) Okadaic acid promotes angiogenesis via activation of hypoxia-inducible factor-1. Cancer Lett 276:102–108. https://doi.org/10.1016/j.canlet.2008.10.034
57. Blum Y, Belting HG, Ellertsdottir E, et al (2008) Complex cell rearrangements during intersegmental vessel sprouting and vessel fusion in the zebrafish embryo. Dev Biol 316:312–322. https://doi.org/10.1016/j.ydbio.2008.01.038
58. Mentzer SJ, Konerding MA (2014) Intussusceptive angiogenesis: Expansion and remodeling of microvascular networks. Angiogenesis 17:499–509. https://doi.org/10.1007/s10456-014-9428-3
59. Norton KA, Popel AS (2016) Effects of endothelial cell proliferation and migration rates in a computational model of sprouting angiogenesis. Sci Rep 6:. https://doi.org/10.1038/srep36992
60. Andrew DJ, Ewald AJ (2010) Morphogenesis of epithelial tubes: Insights into tube formation, elongation, and elaboration. Dev Biol 341:34–55. https://doi.org/10.1016/j.ydbio.2009.09.024
61. Bryan BA, Dennstedt E, Mitchell DC, et al (2010) RhoA/ROCK signaling is essential for multiple aspects of VEGF-mediated angiogenesis. The FASEB Journal 24:3186–3195. https://doi.org/10.1096/fj.09-145102
62. Valenti L, Rametta R, Dongiovanni P, et al (2008) Increased expression and activity of the transcription factor FOXO1 in nonalcoholic steatohepatitis. Diabetes 57:1355–1362. https://doi.org/10.2337/db07-0714
63. Ibrahim HA, Zakaria SS, El-Batch MM, et al (2022) The Value of SIRT1/FOXO1 Signaling Pathway in Early Detection of Cardiovascular Risk in Children with β-Thalassemia Major. Biomedicines 10:. https://doi.org/10.3390/biomedicines10102601
64. Kaela X, Varberg M, Garretson RO, et al (2018) Transgelin induces dysfunction of fetal endothelial colony-forming cells from gestational diabetic pregnancies. Am J Physiol Cell Physiol 315:502–515. https://doi.org/10.1152/ajpcell.00137.2018.-Fetal
65. Dulak J, Józkowicz A (2005) Anti-Angiogenic and Anti-Inflammatory Effects of Statins: Relevance to Anti-Cancer Therapy. Curr Cancer Drug Targets 5:579–594. https://doi.org/10.2174/156800905774932824.
66. Xiao Y, Li Y, Han J, et al (2012) Transgelin 2 Participates in Lovastatin-Induced Anti-Angiogenic Effects in Endothelial Cells through a Phosphorylated Myosin Light Chain-Related Mechanism. PLoS One 7:. https://doi.org/10.1371/journal.pone.0046510

Acknowledgments

We thank M. Tamura, M. Sato, M. Funahashi, T. Simizu, and N. Fujita at Graduate School of Dental Medicine, Hokkaido University, and T. Kotani and M. Miura at the School of Science, Hokkaido University, and M. Fujita at the Faculty of Science, Kanagawa University, for supporting the fish experiments. We thank all the members of the Department of Cell Differentiation and the Liaison Laboratory Research Promotion Center, Institute of Molecular Embryology and Genetics, Kumamoto University.

Funding

This work was supported by the Japan Society for the Promotion of Science (JSPS; grant numbers KAKENHI 15K1125905, 18K0978208, and 22K1018602).

Authorship contributions

K.T-T. developed the research plans, performed the experiments, and did data analysis. M.O. supervised the project. K.T-T. and M.O. discussed the results and wrote the manuscript.

Statements and Declarations

Competing interests

The authors declare that they have no competing interests.

Data availability

The datasets obtained during this study are available from the corresponding author upon reasonable request.

Fig. 1

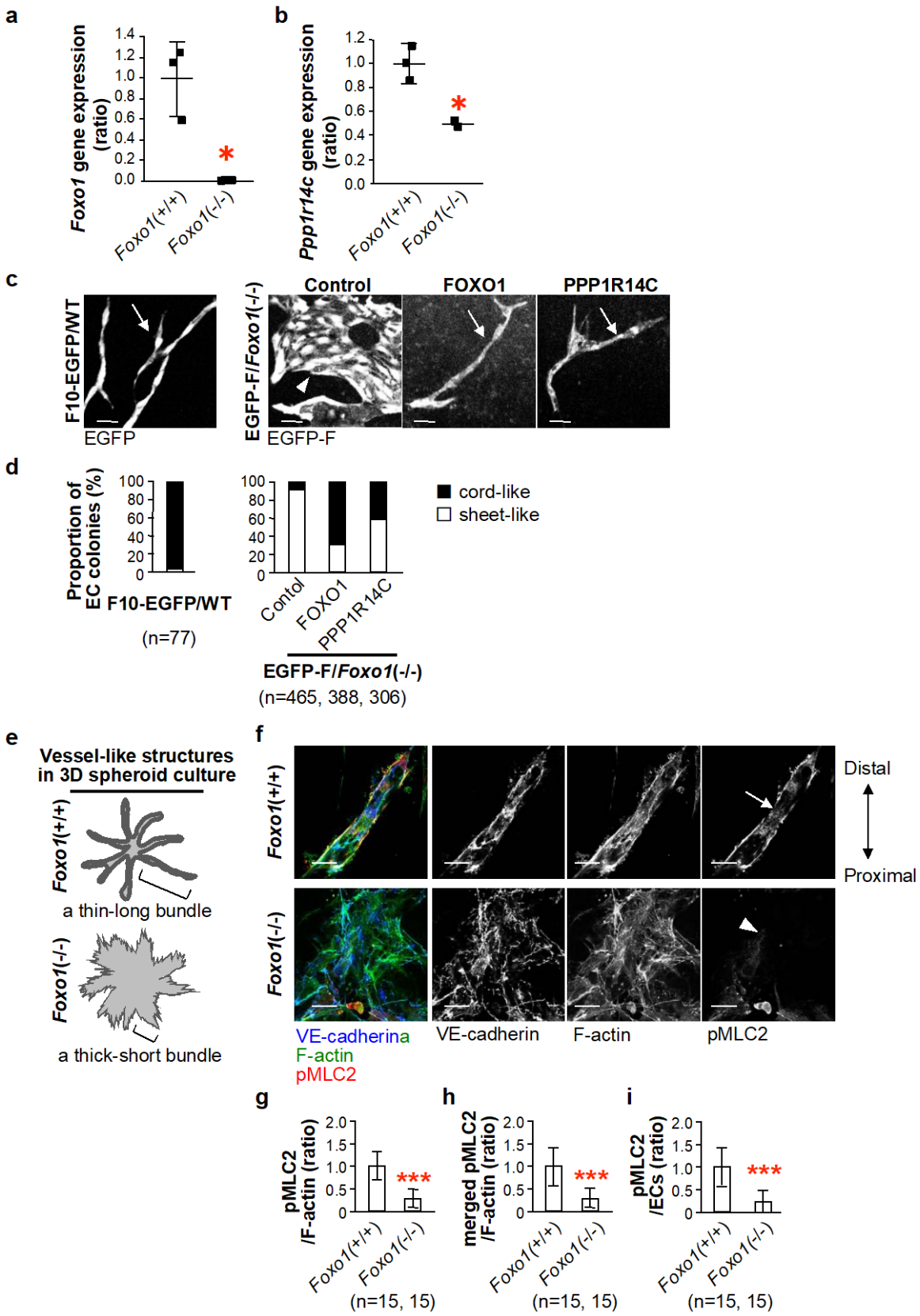
a
Foxo1 gene expression (ratio)
Foxo1(+/+)
Foxo1(-/-)
b
Ppp1r14c gene expression (ratio)
c
F10-EGFP/WT
EGFP
EGFP-F/Foxo1(-/-)
Control
FOXO1
PPP1R14C
EGFP-F
d
Proportion of EC colonies (%)
F10-EGFP/WT
(n=77)
cord-like
sheet-like
Contol
FOXO1
PPP1R14C
EGFP-F/Foxo1(-/-)
(n=465, 388, 306)
e
Vessel-like structures in 3D spheroid culture
Foxo1(+/+)
a thin-long bundle
Foxo1(-/-)
a thick-short bundle
f
Distal
Proximal
VE-cadherina
F-actin
pMLC2
VE-cadherin
F-actin
pMLC2
g
pMLC2 /F-actin (ratio)
(n=15, 15)
h
merged pMLC2 /F-actin (ratio)
(n=15, 15)
i
pMLC2 /ECs (ratio)
(n=15, 15)

Fig. 1 PPP1R14C restores the abnormal morphology of *Foxo1*$^{-/-}$ ECs.
(a and b) *Foxo1*$^{+/+}$ or *Foxo1*$^{-/-}$ mouse embryonic stem cells (ESCs) were cultured on an OP9 stromal cell layer in the presence of VEGF-A165 (10 ng/ml). After 6.5 days, VE-cadherin^{+} CD31^{+} vascular endothelial cells (ECs) were purified by FACS and subjected to an mRNA expression analysis using real-time PCR. The expression level of the target genes was normalized to the expression of b2 microglobulin (*B2m*) and presented as a fold change relative to *Foxo1*$^{+/+}$ ECs (n=3 from three independent experiments using one ESC clone for each genotype). Data were analyzed using an *F*-test, followed by an unpaired two-tailed *t* test (**P*<0.05). (c and d) VE-cadherin^{+} CD31^{+} ECs derived from F10-EGFP ESCs (F10-EGFP/WT) or EGFP-F/*Foxo1*$^{-/-}$ ESCs expressing mouse *Foxo1*, human *PPP1R14C*, or an empty vector (Control) were cultured on an OP9 stromal cell layer in the presence of VEGF-A165 (10 ng/ml) for 3–4 days. (c) Fluorescence images of EC colonies were obtained using confocal microscopy. Arrows indicate cord-like EC colonies, and the arrowhead indicates a sheet-like EC colony. Scale bars indicate 50 μm. (d) The percentage of the two types of EC colonies. The total number of EC colonies examined in three independent experiments using the same clones is indicated in the brackets. (e-i) Flk1^{+} mesodermal cells derived from *Foxo1*$^{+/+}$ or *Foxo1*$^{-/-}$ ESCs were sorted, aggregated, and cultured in a type I collagen gel in the presence of VEGF-A165 (10 ng/ml) for 4–5 days to induce vessel-like structures (3D spheroid culture). (e) Diagrammatic illustration of vessel-like structures. ECs sprouting from aggregates of *Foxo1*$^{+/+}$ mesodermal cells form thin-long elongated vessel-like structures, while *Foxo1*$^{-/-}$ ECs form thick-short bundle structures. (f) Representative confocal images of vessel-like structures immunostained for VE-cadherin (blue), F-actin (green), and phosphorylated myosin light chain 2 (pMLC2) (red) as shown in merged or separated channels. The arrow indicates an elongated EC bundle expressing pMLC2 mainly along the cell circumference. The arrowhead indicates an abnormally shaped EC bundle with no signals of pMLC2 staining, except for cells proximal to the body of the aggregate. The double-headed arrow indicates the orientation of the EC bundle (proximal to distal). Scale bars indicate 20 μm. (g) The ratio of the total area of pMLC2 to the total area of F-actin. (h) The ratio of the area of the merged region of pMLC2 and F-actin to the total area of F-actin. (i) The ratio of the total area of pMLC2 to the total area of ECs. The total number of vessel-like structures examined in five independent experiments using the same clones is indicated in the brackets. Data were analyzed using an *F*-test, followed by an unpaired two-tailed *t* test (****P*<0.001).

Fig. 2

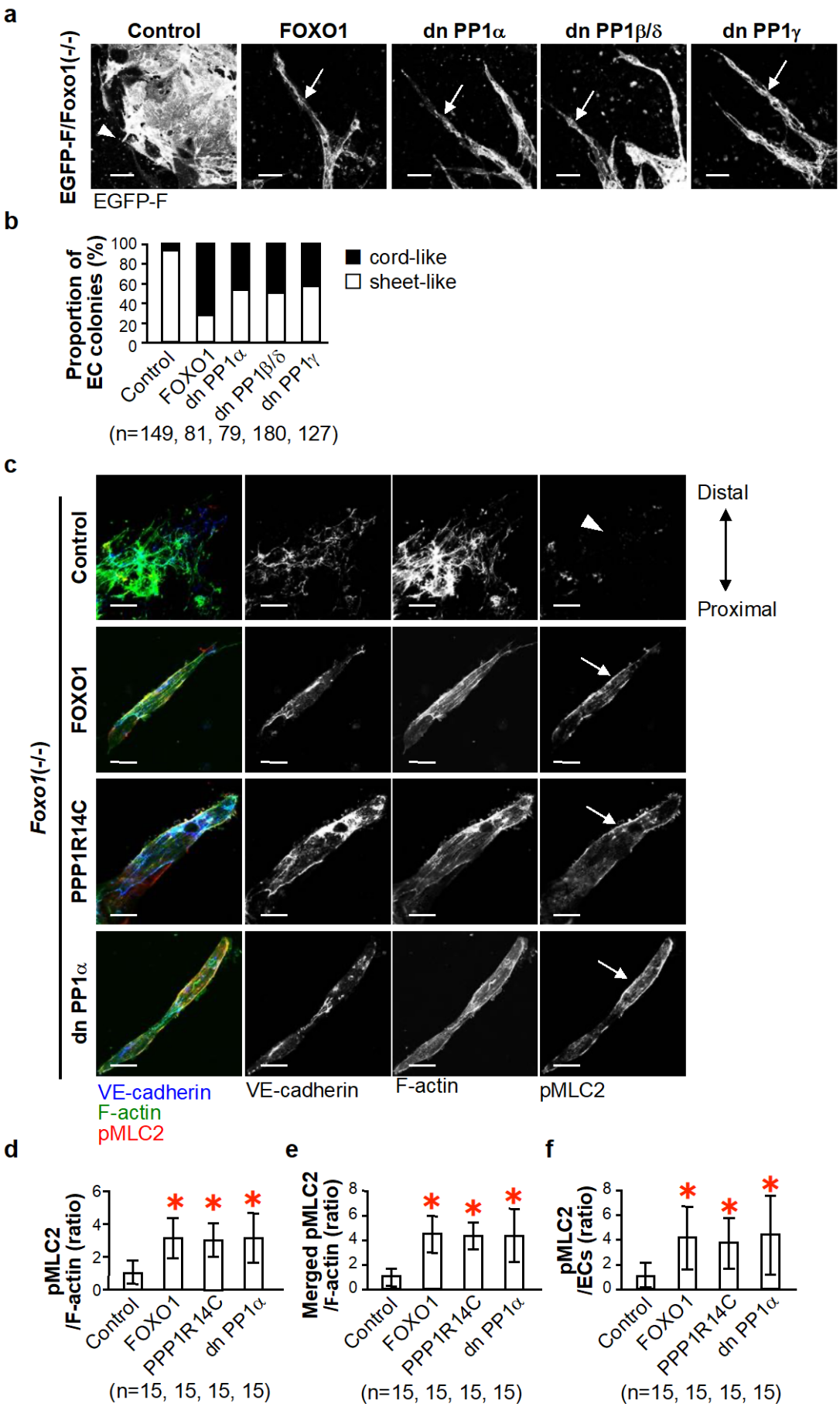
a
Control
FOXO1
dn PP1α
dn PP1β/δ
dn PP1γ
EGFP-F/Foxo1(-/-)
EGFP-F
b
Proportion of EC colonies (%)
100
80
60
40
20
0
cord-like
sheet-like
Control
FOXO1
dn PP1α
dn PP1β/δ
dn PP1γ
(n=149, 81, 79, 180, 127)
c
Foxo1(-/-)
Control
FOXO1
PPP1R14C
dn PP1α
Distal
Proximal
VE-cadherin
F-actin
pMLC2
VE-cadherin
F-actin
pMLC2
d
pMLC2 /F-actin (ratio)
Control
FOXO1
PPP1R14C
dn PP1α
(n=15, 15, 15, 15)
e
Merged pMLC2 /F-actin (ratio)
Control
FOXO1
PPP1R14C
dn PP1α
(n=15, 15, 15, 15)
f
pMLC2 /ECs (ratio)
Control
FOXO1
PPP1R14C
dn PP1α
(n=15, 15, 15, 15)

923

Fig. 2 Dominant-negative PP1 recovers MLC2 phosphorylation and the abnormal morphology of *Foxo1*$^{-/-}$ ECs. (a and b) VE-cadherin^{+} CD31^{+} ECs derived from EGFP-F/*Foxo1*$^{-/-}$ ESCs expressing mouse FOXO1, human dominant-negative (dn) PP1α, dn PP1β/δ or dn PP1γ were cultured on an OP9 stromal cell layer in the presence of VEGF-A165 (10 ng/ml) for 3–4 days. (a) Fluorescence images of EC colonies were obtained using confocal microscopy. The arrowhead indicates a sheet-like EC colony, and arrows indicate cord-like EC colonies. Scale bars indicate 50 μm. (b) The percentage of the two types of EC colonies. The total number of EC colonies examined in three independent experiments using the same clones is indicated in the brackets. (c–f) Flk1^{+} mesodermal cells derived from *Foxo1*$^{-/-}$ ESCs expressing mouse FOXO1, human PPP1R14C, or dn PP1α were aggregated and cultured in a type I collagen gel in the presence of VEGF-A165 (10 ng/ml) for 4–5 days. (c) Vessel-like structures were immunostained for VE-cadherin (blue), F-actin (green), and pMLC2 (red), and confocal images were obtained. The arrowhead indicates an abnormally shaped EC bundle with no signals of pMLC2. Arrows indicate elongated ECs expressing pMLC2 mainly along the cell circumference. The double-headed arrow indicates the orientation of the vessel-like structure (proximal to distal). Scale bars indicate 20 μm. (d) The ratio of the total area of pMLC2 to the total area of F-actin. (e) The ratio of the area of the merged region of pMLC2 and F-actin to the total area of F-actin. (f) The ratio of the total area of pMLC2 to the total area of ECs. The total number of vessel-like structures examined in three independent experiments using the same clones is indicated in the brackets. Data were analyzed using Dunnett's test (*P<0.05 significantly different from the control).

Fig. 3

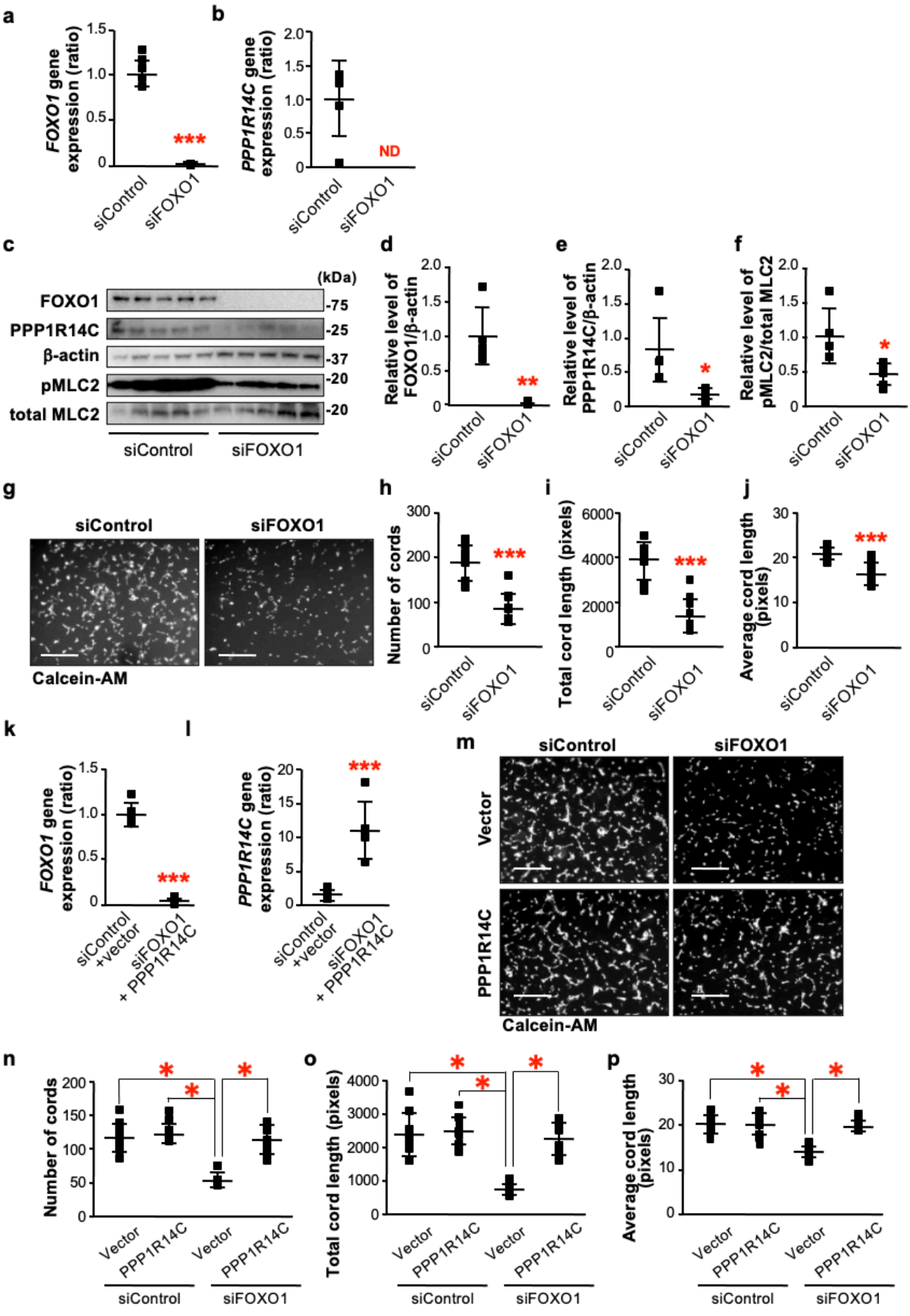
a
FOXO1 gene expression (ratio)
1.5
1.0
0.5
0
***
siControl
siFOXO1
b
PPP1R14C gene expression (ratio)
2.0
1.5
1.0
0.5
0
ND
siControl
siFOXO1
c
(kDa)
FOXO1
PPP1R14C
β-actin
pMLC2
total MLC2
-75
-25
-37
-20
-20
siControl
siFOXO1
d
Relative level of FOXO1/β-actin
2.0
1.5
1.0
0.5
0
**
siControl
siFOXO1
e
Relative level of PPP1R14C/β-actin
2.0
1.5
1.0
0.5
0
*
siControl
siFOXO1
f
Relative level of pMLC2/total MLC2
2.0
1.5
1.0
0.5
0
*
siControl
siFOXO1
g
siControl
siFOXO1
Calcein-AM
h
Number of cords
300
200
100
0
***
siControl
siFOXO1
i
Total cord length (pixels)
6000
4000
2000
0
***
siControl
siFOXO1
j
Average cord length (pixels)
30
20
10
0
***
siControl
siFOXO1
k
FOXO1 gene expression (ratio)
1.5
1.0
0.5
0
***
siControl +vector
siFOXO1 + PPP1R14C
l
PPP1R14C gene expression (ratio)
20
15
10
5
0
***
siControl +vector
siFOXO1 + PPP1R14C
m
siControl
siFOXO1
Vector
PPP1R14C
Calcein-AM
n
Number of cords
200
150
100
50
0
*
*
*
Vector
PPP1R14C
Vector
PPP1R14C
siControl
siFOXO1
o
Total cord length (pixels)
4000
3000
2000
1000
0
*
*
*
Vector
PPP1R14C
Vector
PPP1R14C
siControl
siFOXO1
p
Average cord length (pixels)
30
20
10
0
*
*
*
Vector
PPP1R14C
Vector
PPP1R14C
siControl
siFOXO1

943

Fig. 3 *FOXO1*-knockdown in HUVECs reduces PPP1R14C expression and MLC2 phosphorylation and suppresses angiogenesis.

(a-j) Human umbilical vein endothelial cells (HUVECs) were transfected with siRNA targeting *FOXO1* (siFOXO1) to reduce gene expression. Parallel cultures were transfected with the same amount of control siRNA (siControl). (a and b) The expression levels of *FOXO1* (a) and *PPP1R14C* (b) genes were measured using real-time quantitative PCR. Expression levels were normalized to *ACTB*. Data are presented as a ratio relative to the control (n=5 from five independent experiments). Results were analyzed using an *F*-test, followed by an unpaired two-tailed *t* test (***$P<0.001$). *ND* not detected. (c–f) A Western blot analysis with antibodies against FOXO1, PPP1R14C, b-actin, pMLC2, and total MLC2. (c) Western blot images. (d–f) Expression levels were normalized to b-actin (d and e) or total MLC2 (f). Data are presented as a ratio relative to the control (n=5 from five independent experiments). Results were analyzed using an *F*-test, followed by an unpaired two-tailed *t* test (*$P<0.05$, **$P<0.01$). (g–j) Vascular cord formation by HUVECs in a type I collagen gel sandwich culture. (g) Representative calcein-AM fluorescent images of cord structures. Scale bars indicate 500 μm. (h–j) The number (h) and total length (i) of cord structures and the average cord length (j) per field were examined after 2 days of culture (n=10 fields per group). Results were analyzed by an *F*-test, followed by an unpaired two-tailed *t* ttest (***$P<0.001$). Similar results were obtained in three independent experiments. (k-p) HUVECs were co-transfected with *FOXO1* siRNA (siFOXO1) and human *PPP1R14C*-expressing plasmids (PPP1R14C). Parallel cultures were transfected with the same amount of control siRNA (siControl) and pCAGIPuro vector control (Vector). (k and l) The expression levels of the *FOXO1* (k) and *PPP1R14C* (l) genes were assessed using real-time quantitative PCR. Expression levels were normalized to *ACTB*. Data are presented as a ratio relative to the control (n=5 from five independent experiments). Results were analyzed by an *F*-test, followed by an unpaired two-tailed *t* test (***$P<0.001$). (m–p) Vascular cord formation by HUVECs in a type I collagen gel sandwich culture. (m) Representative calcein-AM fluorescent images of cord structures. Scale bars indicate 500 μm. (n–p) The number (n) and total length (o) of cord structures and the average cord length (p) per field were examined after 2 days of culture (n=10 fields per group). Results were analyzed by Tukey's test (*$P<0.05$). Similar results were obtained in three independent experiments.

Fig. 4

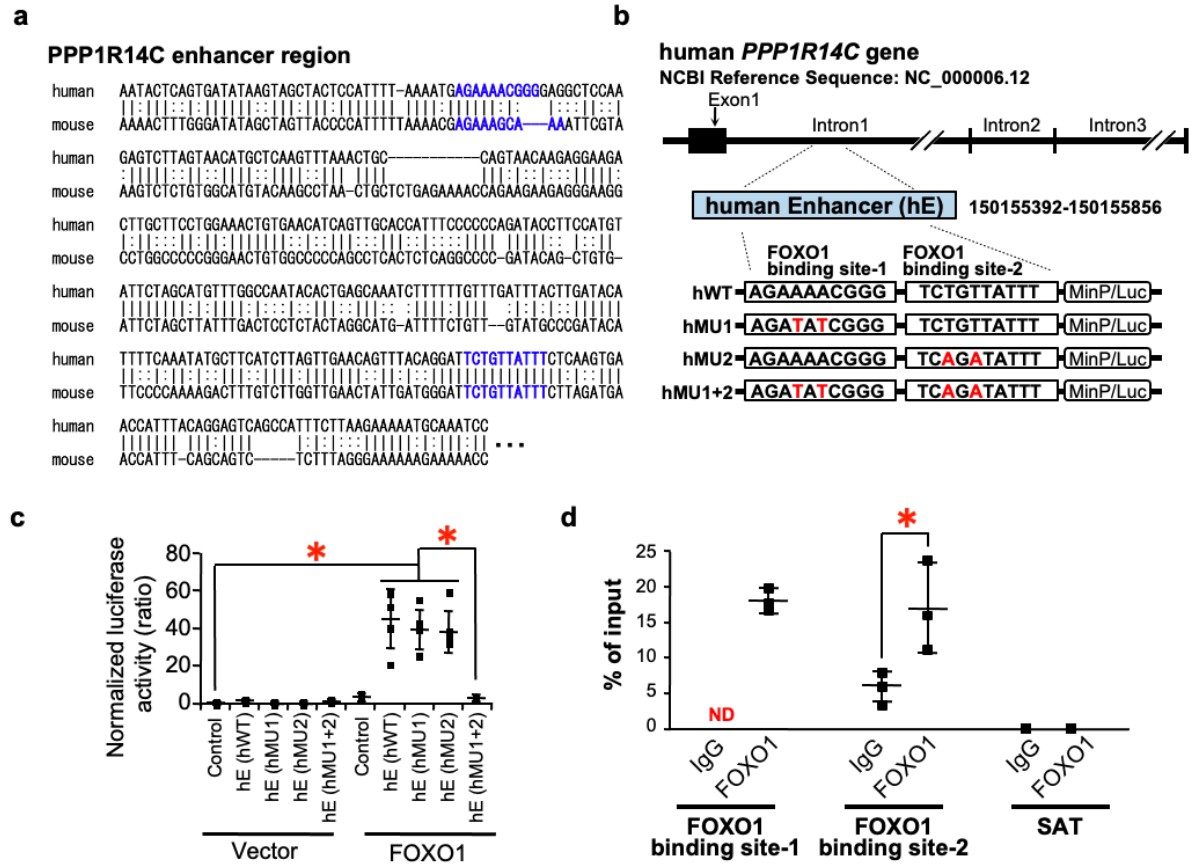

Fig. 4 FOXO1 activates the enhancer element located in the first intron of the human *PPP1R14C* gene. (a) Aligned sequence of the putative enhancer region conserved in the mouse and human *PPP1R14C* genes. Two conserved FOXO1 binding sites are highlighted in blue. (b) Diagram of the putative human enhancer region (hE) containing two FOXO1 binding sites located in the first intron of the human *PPP1R14C* gene. The base numbers indicate the location of hE at the starting and ending points. Lower panels depict the structure of reporter constructs containing the two FOXO1 binding sites (FOXO1 binding sites-1 and -2), in which the consensus sequences are unmodified (hWT) or modified in several ways (hMU1, hMU2, and hMU1+2). Mutations are highlighted in red. MinP and Luc indicate a minimal promoter and the firefly luciferase gene, respectively. (c) Luciferase reporter assay of the enhancer activity of hE. HUVECs were co-transfected with a Renilla luciferase vector (pRL-SV40), firefly luciferase vector, and pCAGIPuro vector with or without the mouse *Foxo1* gene (FOXO1). Luciferase activities were measured one day after transfection. Data are presented as ratios of luciferase activities to the control [pGL empty vector (Control) plus pCAGIPuro empty vector (Vector)]. Results were analyzed using Tukey's test (n=5, *$P<0.05$). Similar results were obtained in three independent experiments. (d) CUT&RUN assay using HUVECs with an anti-FOXO1 antibody and real-time PCR assay of FOXO1 binding site-1 and FOXO1 binding site-2 in hE. IgG is an isotype control. Alpha satellite repeat (SAT) is a negative control. Results were analyzed using an *F*-test, followed by an unpaired two-tailed *t* test (n=3, *$P<0.05$). *ND* not detected. Similar results were obtained in three independent experiments.

Fig. 5

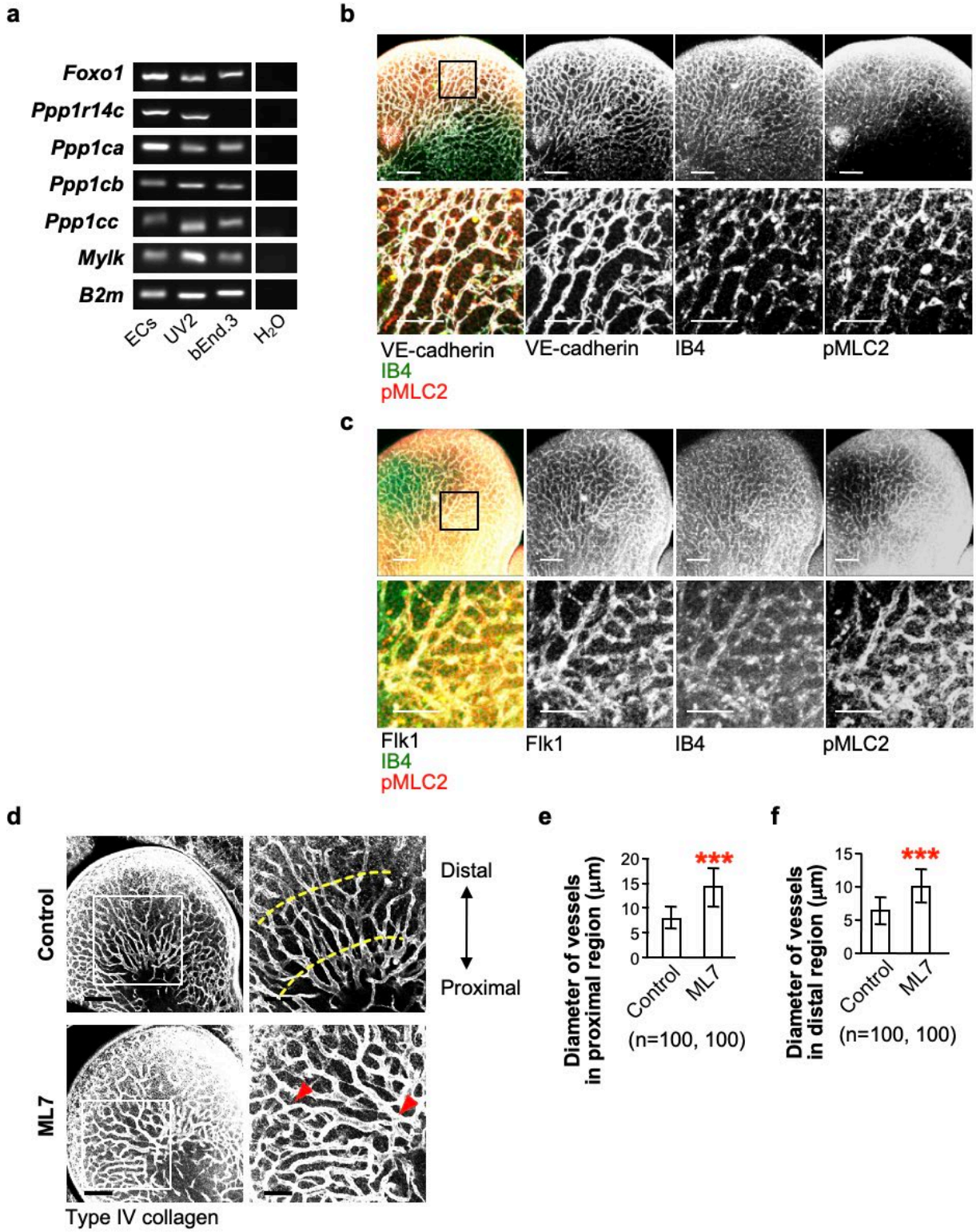
a
Foxo1
Ppp1r14c
Ppp1ca
Ppp1cb
Ppp1cc
Mylk
B2m
ECs
UV2
bEnd.3
H2O
b
VE-cadherin
IB4
pMLC2
VE-cadherin
IB4
pMLC2
c
Flk1
IB4
pMLC2
Flk1
IB4
pMLC2
d
Control
ML7
Distal
Proximal
Type IV collagen
e
Diameter of vessels in proximal region (μm)
***
Control
ML7
(n=100, 100)
f
Diameter of vessels in distal region (μm)
***
Control
ML7
(n=100, 100)

Fig. 5 MLCK-inhibition causes an abnormal vascular structure in mouse embryos.
(a) The mRNA expression of *Foxo1*, *Ppp1r14c*, *Ppp1ca*, *Ppp1cb*, *Ppp1cc*, and *Mylk* in VE-cadherin^{+} Flk1^{+} CD31^{+} CD45^{-} ECs sorted from E10.5 mouse embryos and the mouse EC lines, UV2 and bEnd.3, was detected using RT-PCR. *B2m* expression as an internal control and no-template negative control (H_2O) are shown. Similar results were obtained from three independent experiments using different batches of collected cells. (b) Representative confocal images of the forelimb vessels of E11.5 mouse embryos whole-mount immunostained for VE-cadherin (white), isolectin B4 (IB4, green), and pMLC2 (red), shown in merged or separated channels. Lower panels show a higher magnification of the boxed area in each upper panel. Scale bars indicate 100 μm (upper panels) or 50 μm (lower panels). Similar results were obtained from three independent experiments using embryos of different litters. (c) Representative confocal images of forelimb vessels were the same as in (b), except that VE-cadherin was replaced by Flk1 (white). (d–f) Pregnant ICR mice were intraperitoneally injected with ML7 (13.58 mg/kg body weight) or DMSO as a vehicle control once a day at E8.5, E9.5, and E10.5. (d) The forelimb vessels of E11.5 mouse embryos were investigated by whole-mount immunostaining for Type IV collagen. Right panels show a higher magnification of the boxed area in each left panel. Yellow dot lines indicate the position of vessels (proximal and distal) measured in (e) and (f). Red arrowheads indicate abnormally thick and dilated vessels. Scale bars indicate 100 μm (left panels) or 50 μm (right panels). Similar results were obtained from three independent experiments using embryos of different litters. (e and f) Diameters of the vessels in the proximal region (e) and distal region (f). The total number of vessels examined in 20 embryos in three independent experiments is indicated in the brackets. Data were analyzed using an *F*-test, followed by an unpaired two-tailed *t test* (***P<0.001).

Fig. 6

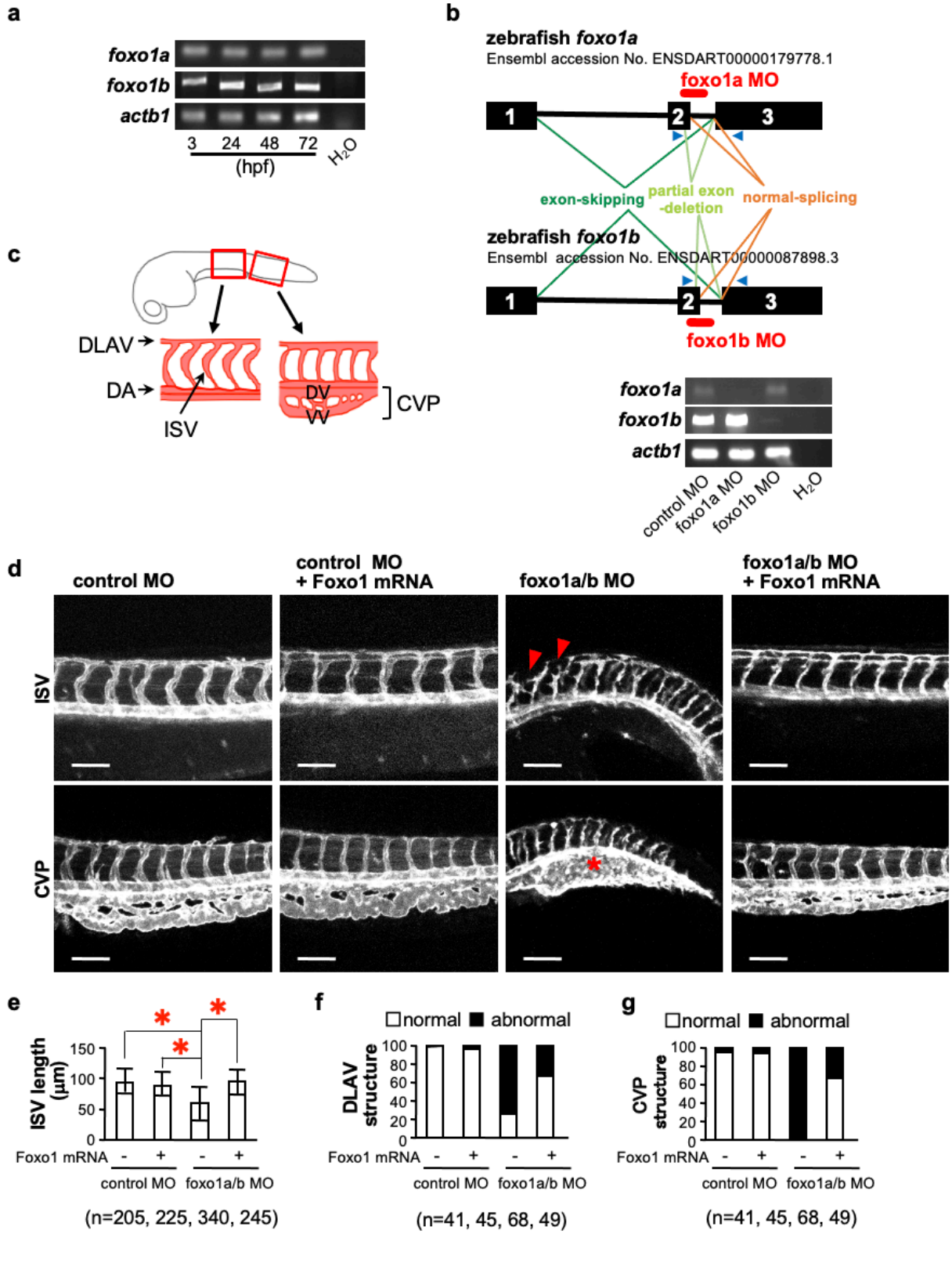
a
foxo1a
foxo1b
actb1
3 24 48 72 H2O
(hpf)
b
zebrafish foxo1a
Ensembl accession No. ENSDART00000179778.1
foxo1a MO
1 2 3
exon-skipping
partial exon -deletion
normal-splicing
zebrafish foxo1b
Ensembl accession No. ENSDART00000087898.3
1 2 3
foxo1b MO
foxo1a
foxo1b
actb1
control MO
foxo1a MO
foxo1b MO
H2O
c
DLAV
DA
ISV
DV
VV
CVP
d
control MO
control MO + Foxo1 mRNA
foxo1a/b MO
foxo1a/b MO + Foxo1 mRNA
ISV
CVP
e
ISV length (μm)
150
100
50
0
Foxo1 mRNA - + - +
control MO
foxo1a/b MO
(n=205, 225, 340, 245)
f
normal
abnormal
DLAV structure
100
80
60
40
20
0
Foxo1 mRNA - + - +
control MO
foxo1a/b MO
(n=41, 45, 68, 49)
g
normal
abnormal
CVP structure
100
80
60
40
20
0
Foxo1 mRNA - + - +
control MO
foxo1a/b MO
(n=41, 45, 68, 49)

Fig. 6 *foxo1*-knockdown causes an abnormal vascular structure in zebrafish embryos.
(a) *foxo1a* and *foxo1b* mRNA expression in *Tg(fli1a:Myr-mCherry)* zebrafish embryos of the indicated hours post-fertilization (hpf) were detected using RT-PCR. *actb1* as an internal control and no-template negative control (H_2O) are shown. Similar results were obtained from three independent experiments. (b) Partial structures of zebrafish *foxo1a* and *foxo1b* pre-mRNA. Black rectangles and bars indicate coding exons (exon number in white) and introns. Red bars indicate the targets of antisense morpholino oligonucleotides (MO) blocking the splice site of second exon and second intron. Possible splicing outcomes are as follows: normal-splicing (orange), exon-skipping (green), and partial exon-deletion (light green). Blue arrowheads indicate the primers to confirm the MO effects by RT-PCR. Representative results in morphants are shown in the lower panel. *actb1* was amplified as an internal control. Control morphants showed the products expected from normal-splicing. No corresponding product was detected in *foxo1a* or *foxo1b* morphants, suggesting exon-skipping or partial-deletion. Similar results were obtained from three independent experiments. (c) Schematic diagram of the vasculature in the middle trunk and tail regions of zebrafish embryos. DLAV: dorsal longitudinal anastomotic vessel, DA: dorsal aorta, ISV: intersegmental vessel, DV: dorsal vein, VV: ventral vein, CVP: caudal vein plexus. (d–g) *Tg(fli1a:Myr-mCherry)* zebrafish embryos were injected with control MO (control MO) or a mixture of MO targeting *foxo1a* and *foxo1b* (foxo1a/b MO) (15 ng each, total 30 ng) with or without mouse *Foxo1* mRNA (Foxo1 mRNA) (400 pg). (d) ISVs (upper panels) and CVP (lower panels) were analyzed in 2 days post-fertilization (dpf) embryos. Red arrowheads indicate hypoplastic DLAV, and an asterisk indicates an incompletely remodeled CVP. Scale bars indicate 100 μm. Similar results were obtained in three independent experiments. (e) The length of ISVs. Results were analyzed using Tukey's test (*P<0.05). The total number of ISVs examined in three independent experiments is indicated in the brackets. (f) The ratio of embryos with normal and abnormal DLAV. (g) The ratio of embryos with normal and abnormal CVP. The total number of embryos examined in three independent experiments is indicated in the brackets (f and g).

Fig. 7

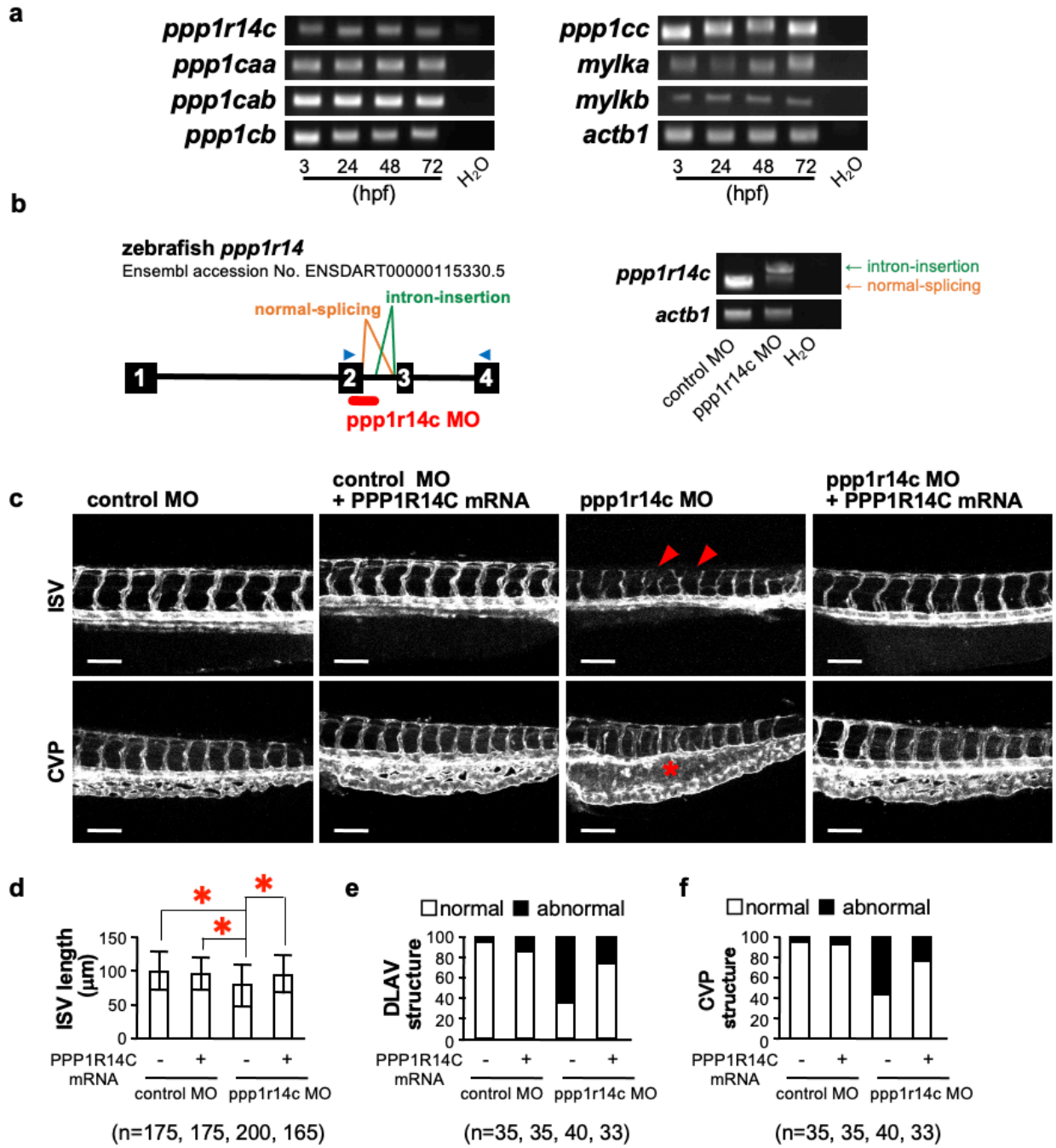
a
ppp1r14c
ppp1caa
ppp1cab
ppp1cb
3 24 48 72 H2O
(hpf)
ppp1cc
mylka
mylkb
actb1
3 24 48 72 H2O
(hpf)
b
zebrafish ppp1r14
Ensembl accession No. ENSDART00000115330.5
normal-splicing
intron-insertion
1 2 3 4
ppp1r14c MO
ppp1r14c
actb1
← intron-insertion
← normal-splicing
control MO
ppp1r14c MO
H2O
c
control MO
control MO
+ PPP1R14C mRNA
ppp1r14c MO
ppp1r14c MO
+ PPP1R14C mRNA
ISV
CVP
d
ISV length (μm)
150
100
50
0
PPP1R14C mRNA
- + - +
control MO
ppp1r14c MO
(n=175, 175, 200, 165)
e
normal abnormal
DLAV structure
100
80
60
40
20
0
PPP1R14C mRNA
- + - +
control MO
ppp1r14c MO
(n=35, 35, 40, 33)
f
normal abnormal
CVP structure
100
80
60
40
20
0
PPP1R14C mRNA
- + - +
control MO
ppp1r14c MO
(n=35, 35, 40, 33)

Fig. 7 *ppp1r14c*-knockdown causes an abnormal vascular structure in zebrafish embryos.
(a) The mRNA expression of the genes regulating MLC2 phosphorylation in *Tg(fli1a:Myr-mCherry)* zebrafish embryos of the indicated hpf were detected using RT-PCR. *actb1* as an internal control and no-template negative control (H_2O) are shown. Similar results were obtained from three independent experiments. (b) Partial structure of zebrafish *ppp1r14c* pre-mRNA. Black rectangles and bars indicate coding exons and introns, respectively. Numbers in the rectangles indicate exon numbers. The red bar indicates the target of MO that blocks the splice site of the second exon and second intron. Possible splicing outcomes are normal-splicing (orange) and the insertion of the intron (green). Blue arrowheads indicate the primer pairs to confirm the effects of MO by RT-PCR. Representative results of RT-PCR in morphant zebrafish embryos are shown in the right panel. *actb1* was amplified as an internal control. Control morphants showed the amplification products expected from normal-splicing, while a product with a larger size was detected in the *ppp1r14c* morphants, suggesting that the intron insertion occurred. Similar results were obtained from three independent experiments. (c–f) *Tg(fli1a:Myr-mCherry)* zebrafish embryos were injected with control MO (control MO) or ppp1r14c MO (ppp1r14c MO) (7 ng) with or without human *PPP1R14C* mRNA (PPP1R14C mRNA) (400 pg). (c) The structures of ISVs (upper panels) and CVP (lower panels) were analyzed in 2 dpf embryos. Red arrowheads indicate hypoplastic DLAV, and an asterisk indicates an incompletely remodeled CVP. Scale bars indicate 100 μm. Similar results were obtained in three independent experiments. (d) The length of ISVs in the morphants. Results were analyzed using Tukey's test (*P<0.05). The total number of ISVs examined in three independent experiments is indicated in the brackets. (e) The ratio of embryos with normal and abnormal DLAV. (f) The ratio of embryos with normal and abnormal CVP. The total number of embryos examined in three independent experiments is indicated in the brackets (e and f).

Fig. 8

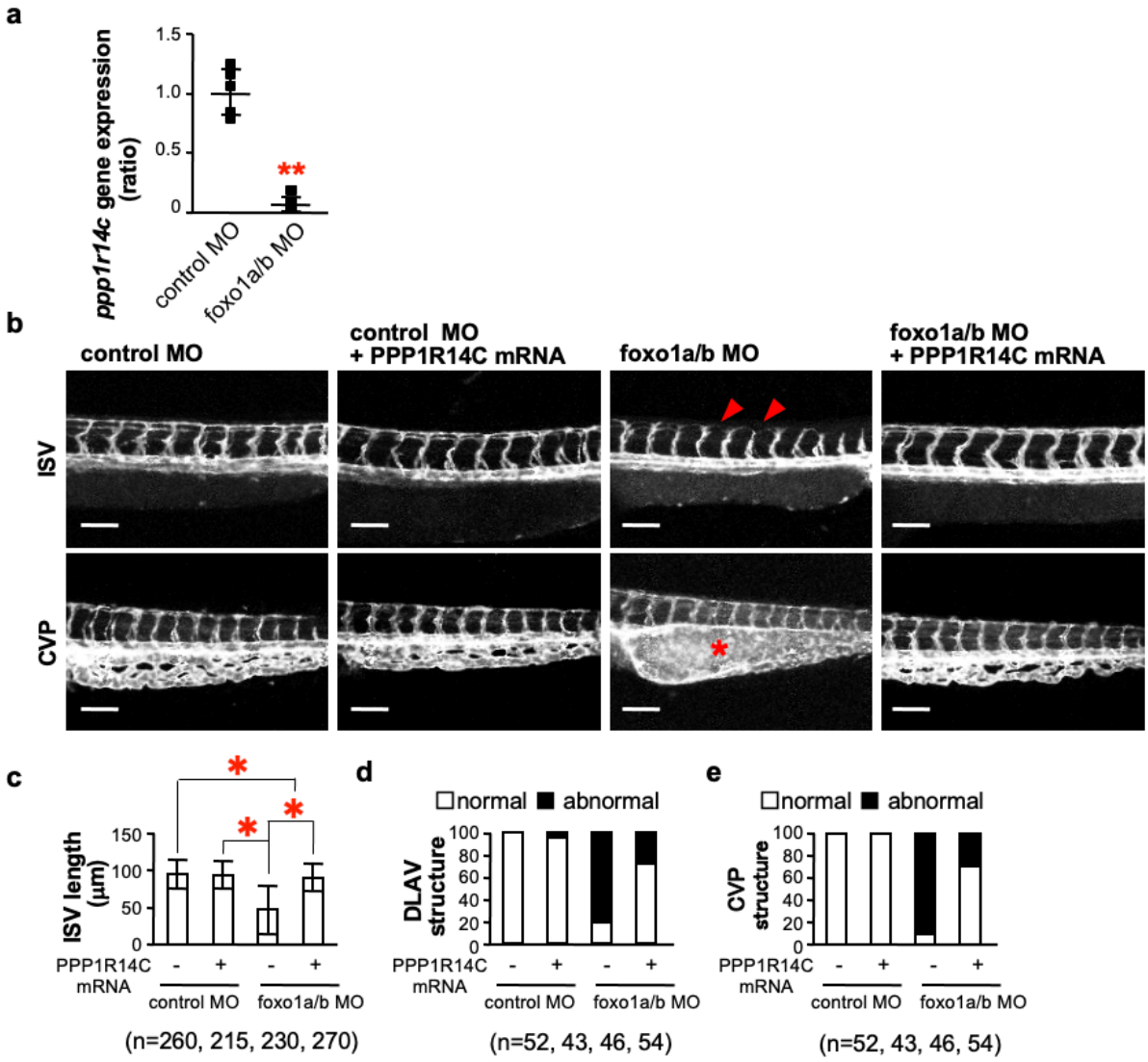

Fig. 8 PPP1R14C-induction restores vascular defects in *foxo1* morphants.

Tg(fli1a:Myr-mCherry) zebrafish embryos were injected with a mixture of MO targeting *foxo1a* and *foxo1b* (foxo1a/b MO) (7 ng each, total 14 ng) with or without human *PPP1R14C* mRNA (PPP1R14C mRNA) (400 pg). (a) The expression of the *ppp1r14c* gene in *foxo1a/b* morphants 2 dpf was detected using real-time quantitative PCR. Expression levels were normalized to that of *actb1*. Data are presented as a ratio relative to the control (n=5 from five independent experiments). Results were analyzed by an *F*-test, followed by an unpaired two-tailed *t test* (***P*<*0*.01). (b) The structures of ISVs (upper panels) and CVP (lower panels) were analyzed in 2 dpf embryos. Red arrowheads indicate hypoplastic DLAV, and an asterisk indicates an incompletely remodeled CVP. Scale bars indicate 100 μm. Similar results were obtained in three independent experiments. (c) The length of ISVs in the morphants. Results were analyzed using Tukey's test (**P*<0.05). The total number of ISVs examined in three independent experiments is indicated in the brackets. (d) The ratio of embryos with normal and abnormal DLAV. (e) The ratio of embryos with normal and abnormal CVP. The total number of embryos examined in three independent experiments is indicated in the brackets (d and e).

Supplementary Information

Title: FOXO1 promotes endothelial cell elongation and angiogenesis by up-regulating the phosphorylation of myosin light chain 2

Journal: Angiogenesis

Authors: Kiyomi Tsuji-Tamura[1]*, and Minetaro Ogawa [2]

Affiliations:
[1]Oral Biochemistry and Molecular Biology, Department of Oral Health Science, Faculty of Dental Medicine and Graduate School of Dental Medicine, Hokkaido University, Kita 13, Nishi 7, Kita-Ku, Sapporo, 060-8586, Japan
[2]Department of Cell Differentiation, Institute of Molecular Embryology and Genetics, Kumamoto University, 2-2-1 Honjo, Chuo-Ku, Kumamoto, 860-0811, Japan

***Author for correspondence:** Kiyomi Tsuji-Tamura, Oral Biochemistry and Molecular Biology, Department of Oral Health Science, Faculty of Dental Medicine and Graduate School of Dental Medicine, Hokkaido University, Kita 13, Nishi 7, Kita-Ku, Sapporo 060-8586, Japan, Tel: +81-11-706-4234, e-mail: ktamuratsuji@den.hokudai.ac.jp, ORCID: 0000-0002-0961-5402

Supplementary Fig. 1

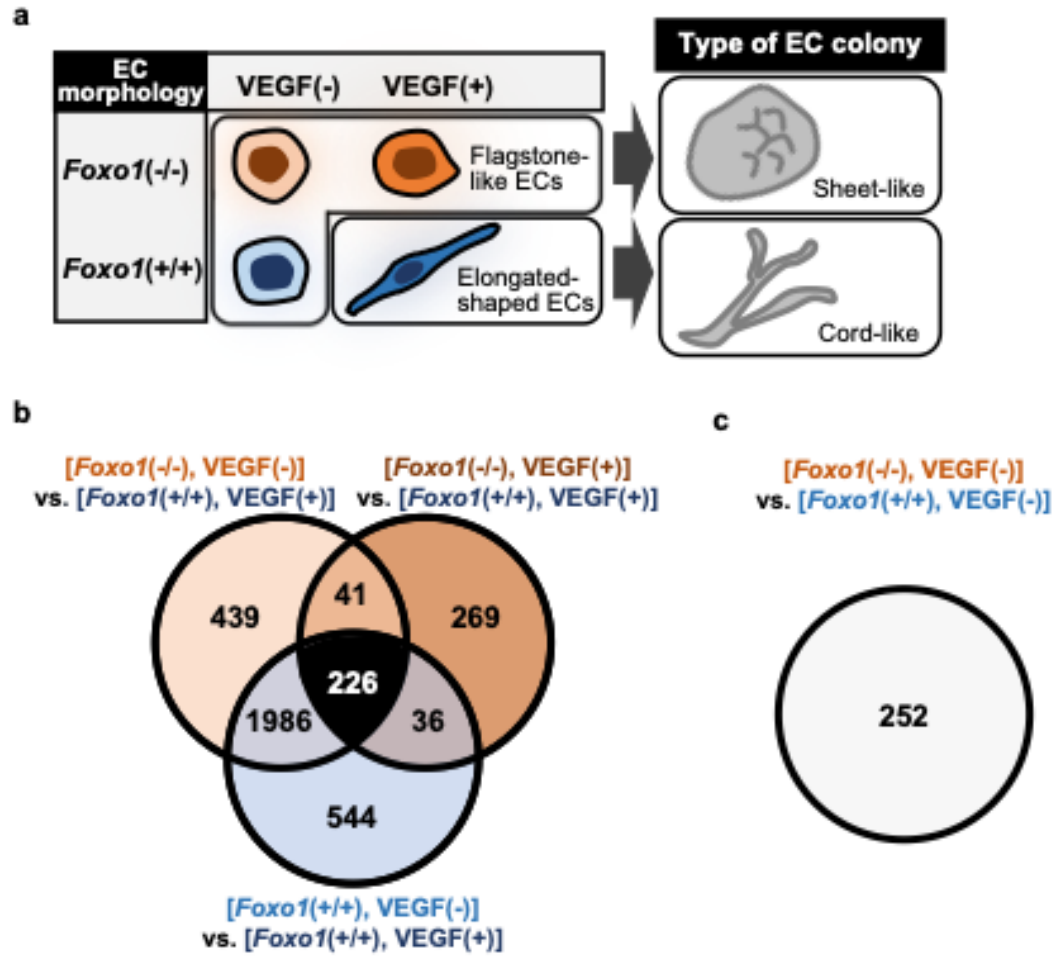

Supplementary Fig. 1 Venn diagram of differentially expressed genes in endothelial cells.
(a) Schematic illustration of the morphology of embryonic stem cells-derived vascular endothelial cells (ESC-ECs) and the type of vascular endothelial cell (EC) colony. *Foxo1*$^{-/-}$ ESC-ECs and *Foxo1*$^{+/+}$ ESC-ECs show a flagstone-like shape and form sheet-like colonies on the OP9 stromal cell layer in the absence of exogenous VEGF-A165. A stimulation with a high concentration of VEGF-A165 (10 ng/ml) induces the elongation of *Foxo1*$^{+/+}$ ESC-ECs, which form long cord-like colonies. In contrast, *Foxo1*$^{-/-}$ ESC-ECs do not elongate, show an abnormal flagstone-like shape, and form abnormal sheet-like colonies in response to exogenous VEGF-A165. (b) Venn diagram of the number of differentially expressed genes (DEGs) in *Foxo1*$^{-/-}$ ESC-ECs in the absence or presence of VEGF-A165 [*Foxo1*(-/-), VEGF(-); *Foxo1*(-/-), VEGF(+)] or *Foxo1*$^{+/+}$ ESC-ECs in the absence of VEGF-A165 [*Foxo1*(+/+), VEGF(-)] relative to *Foxo1*$^{+/+}$ ESC-ECs in the presence of VEGF-A165 [*Foxo1*(+/+), VEGF(+)]. The intersection shown in black indicates the 226 genes commonly reduced in the three flagstone-like EC groups relative to the elongated EC group and, thus, are defined as "EC elongation-related genes (ERGs)". (c) The expression of 252 genes was lower in *Foxo1*$^{-/-}$ ESC-ECs than in *Foxo1*$^{+/+}$ ESC-ECs in the absence of VEGF-A165. They represent Foxo1-dependent genes expressed in steady-state ECs. Notably, most ERGs in (b) are not extracted in the comparison in (c), suggesting that the gene expression landscape is dynamically changing in EC elongation.

Supplementary Fig. 2

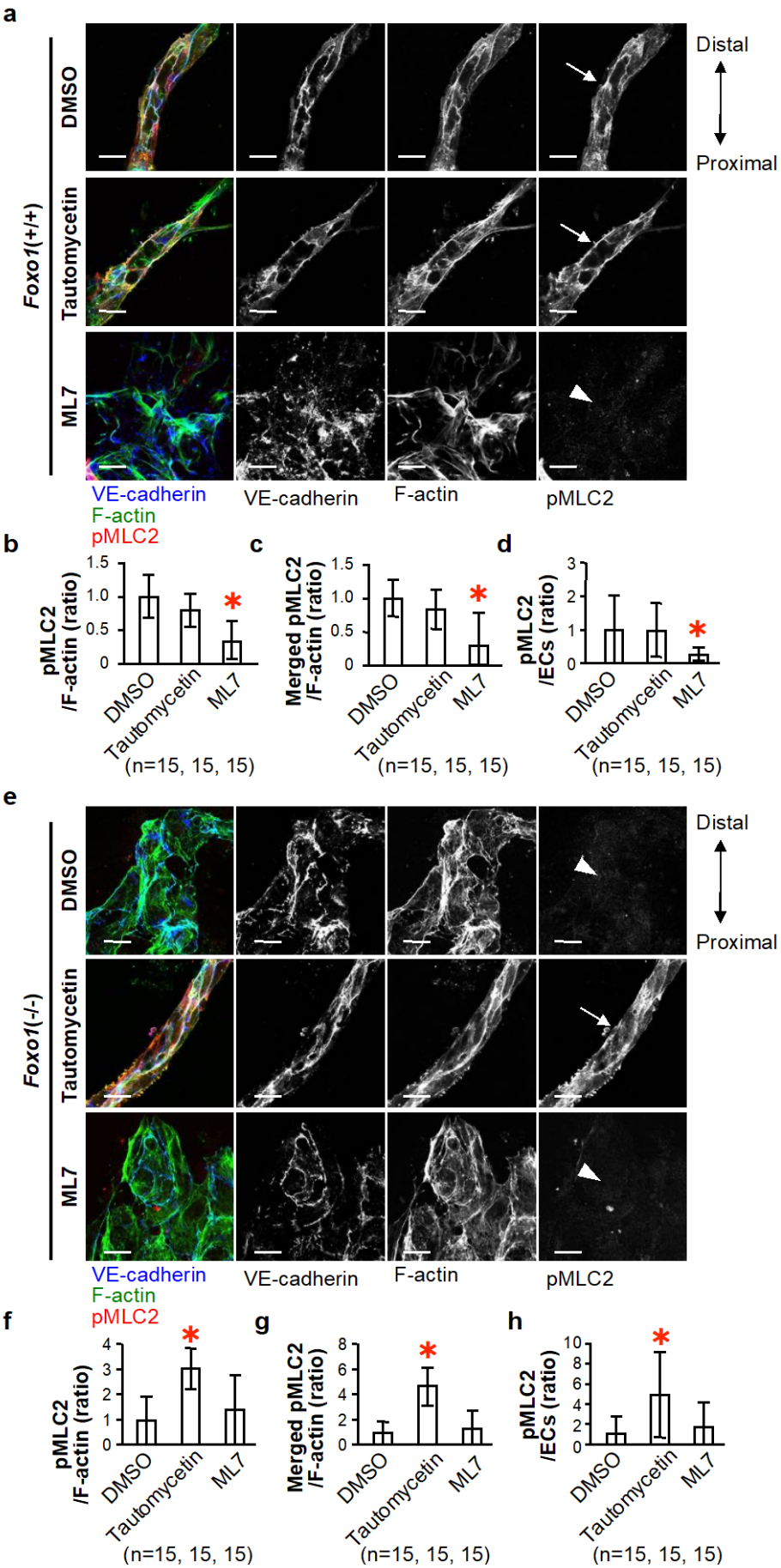

Supplementary Fig. 2 The phosphorylation of MLC2 is required for EC elongation.

Flk1^{+} mesodermal cells derived from *Foxo1*$^{+/+}$ ESCs (a–d) or *Foxo1*$^{-/-}$ ESCs (e–h) were aggregated and cultured in a type I collagen gel in the presence of VEGF-A165 (10 ng/ml). After one day, tautomycetin (5 nmol/L), ML7 (3 μmol/L), or DMSO was added and cultured for 3 days. (a and e) Representative confocal images of vessel-like structures immunostained for VE-cadherin (blue), F-actin (green), and pMLC2 (red). Arrows indicate elongated ECs expressing pMLC2 mainly along the cell circumference. Arrowheads indicate aberrantly shaped ECs with no signals of pMLC2 staining. Double-headed arrows indicate the orientation of the vessel-like structure (proximal to distal). Scale bars indicate 20 μm. Similar results were obtained in three independent experiments using the same clones. (b and f) The ratio of the total area of pMLC2 to the total area of F-actin. (c and g) The ratio of the area of the merged region of pMLC2 and F-actin to the total area of F-actin. (d and h) The ratio of the total area of pMLC2 to the total area of ECs. The total number of vessel-like structures examined in three independent experiments is indicated in the brackets. Data were analyzed using Dunnett's test (*P<0.05 significantly different from the DMSO control).

Supplementary Fig. 3

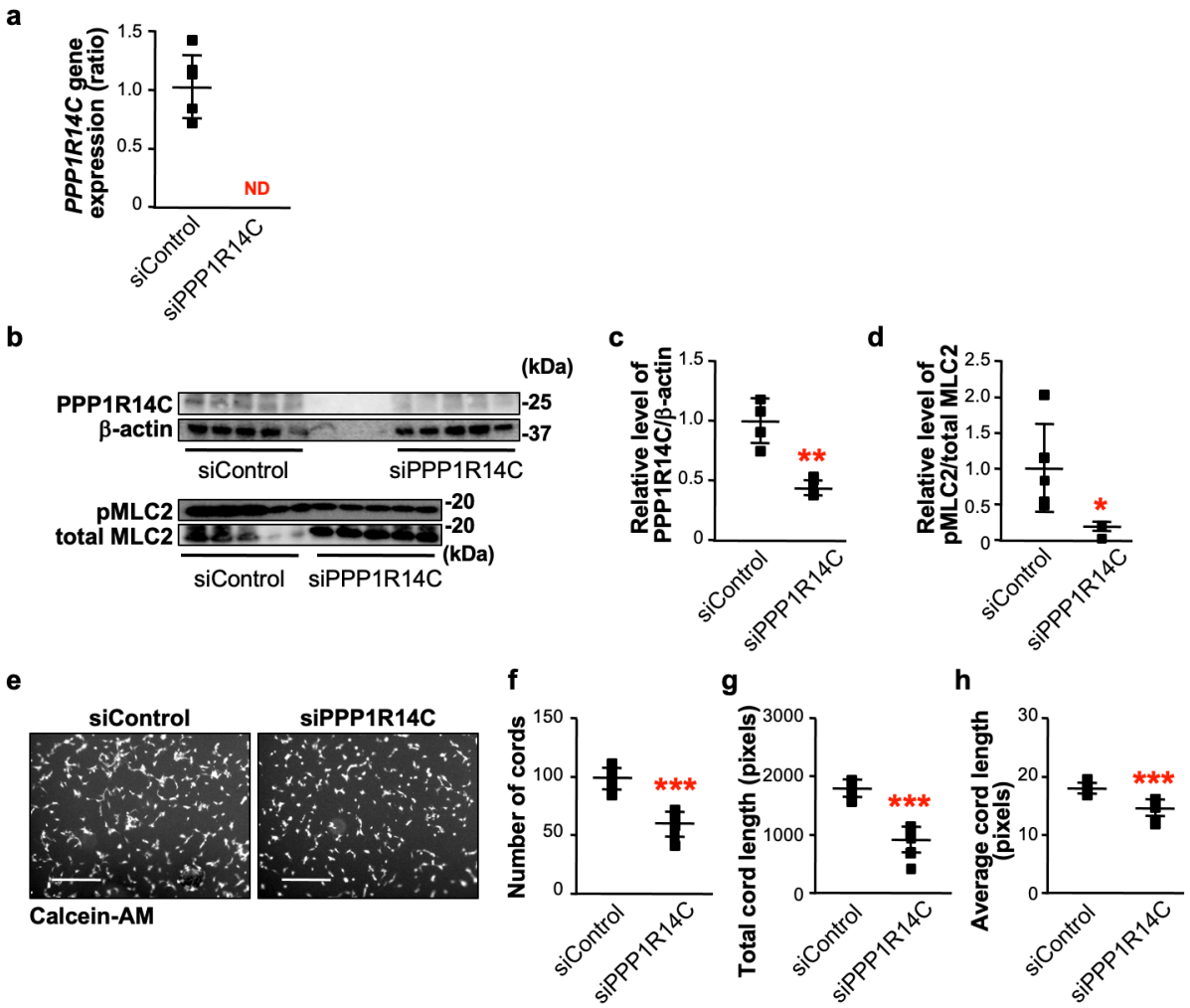

Supplementary Fig. 3 The knockdown of *PPP1R14C* in HUVECs suppresses MLC2 phosphorylation and angiogenesis.

HUVECs were transfected with siRNA targeting *PPP1R14C* (siPPP1R14C) to reduce gene expression. Parallel cultures were transfected with the same amount of control siRNA (siControl). (a) The expression level of the *PPP1R14C* gene was assessed using real-time quantitative PCR. Expression levels were normalized to *ACTB*. Data are presented as a ratio relative to the control (n=5 from five independent experiments). *ND* not detected. (b–d) Western blot analysis with antibodies against PPP1R14C, β-actin, pMLC2, and total MLC2. (b) Western blot images. (c and d) Expression levels were normalized to β-actin (c) and total MLC2 (d). Data are presented as a ratio relative to the control (n=5 from five independent experiments). Results were analyzed by an *F*-test, followed by an unpaired two-tailed *t* test (**P*<0.05, ***P*<0.01). (e–h) Vascular cord formation by HUVECs in a type I collagen gel sandwich culture. (e) Representative calcein-AM fluorescent images of cord structures. Scale bars indicate 500 μm. (f–h) The number (f) and total length (g) of cord structures and the average cord length (h) per field were examined after 2 days of culture (n=10 fields per group). Results were analyzed by an *F*-test, followed by an unpaired two-tailed *t* test (****P*<0.001). Similar results were obtained in three independent experiments.

Supplementary Fig. 4

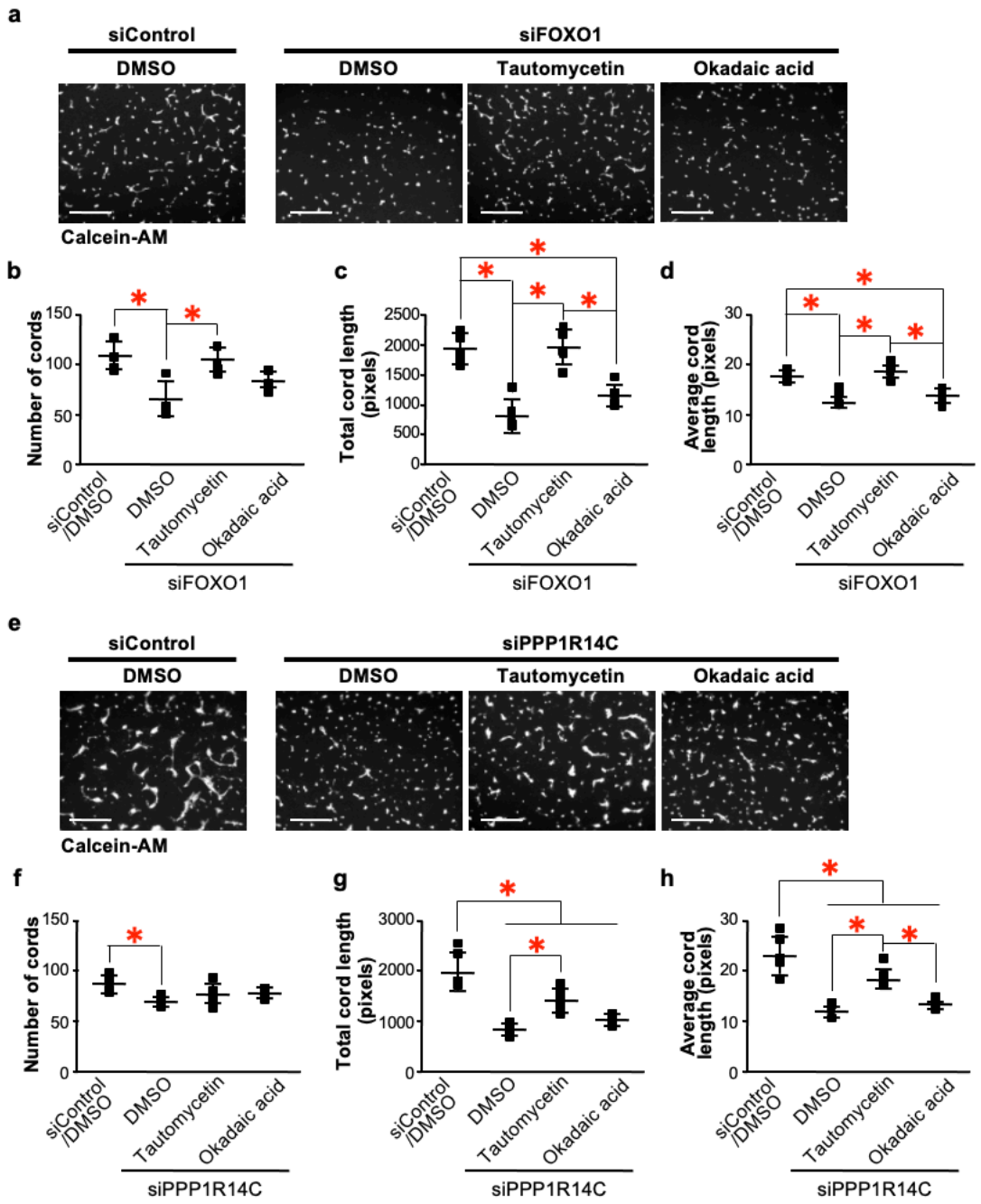

Supplementary Fig. 4 PP1 inhibition by tautomycetin rescues the abnormal morphology of *FOXO1*- or *PPP1R14C*-knockdown in HUVECs.

HUVECs were transfected with *FOXO1* siRNA (siFOXO1) (a-d) or *PPP1R14C* siRNA (siPPP1R14C) (e-h). Parallel cultures were transfected with the same amount of control siRNA (siControl). The cells were cultured in type I collagen sandwich gels, and treated with tautomycetin (1 nmol/L), Okadaic acid (1 nmol/L), or DMSO for 2 days. (a and e) Representative calcein-AM fluorescent images of cord structures. Scale bars indicate 500 μm. (b-d and f-h) The number (b and f) and total length (c and g) of cord structures and the average cord length (d and h) per field were examined after 2 days of culture (n=5 fields per group). Results were analyzed by Tukey's test (*$P<0.05$). Similar results were obtained in three independent experiments.

Supplementary Fig. 5

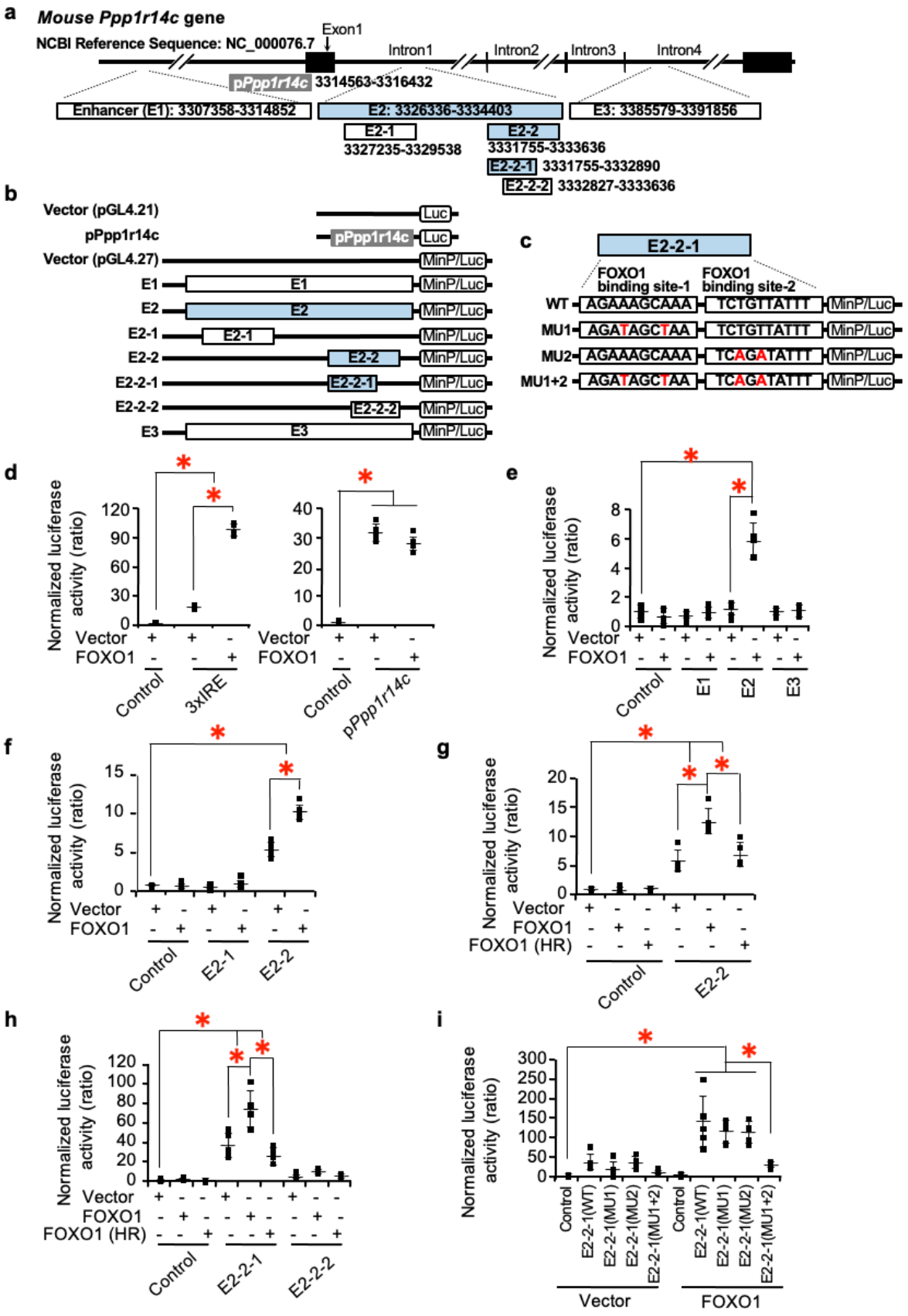

Supplementary Fig. 5 FOXO1 activates the enhancer element located in the first intron of the mouse *Ppp1r14c* gene.

(a) Diagram of the promoter and putative enhancer regions in the mouse *Ppp1r14c* gene. The promoter region and three putative enhancer regions are depicted as p*Ppp1r14c* and E1, E2, and E3, respectively. Base numbers indicate the location of the enhancer regions and their subregions at the starting and ending points. Regions in light blue contain FOXO1-binding sites. (b) Diagram of the plasmid constructs used in reporter assays for the promoter and putative enhancer regions. Luc: the firefly luciferase gene, MinP: minimal promoter. (c) Diagram of the plasmid constructs used in reporter assays for E2-2-1 containing two FOXO1-binding sites (FOXO1-binding sites 1 and 2). The mutations induced in the binding sites are indicated in red. (d–i) Luciferase reporter assay of the *Ppp1r14c* promoter and enhancer activities. The mouse EC line UV2 was co-transfected with the Renilla luciferase vector (pRL-SV40), firefly luciferase vector, and pCAGIPuro vector with or without the mouse *Foxo1* gene (FOXO1). Luciferase activity was measured at 2 days after transfection. Data are presented as the ratios of luciferase activities to the control [pGL empty vector (Control) plus pCAGIPuro empty vector (Vector)]. Results were analyzed using Tukey's test (n=5, **P*<0.05). Similar results were obtained in three independent experiments. Induced FOXO1 activated insulin response elements (3×IRE) (d, left panel). The activity of the *Ppp1r14c* promoter was independent of FOXO1 (d, right panel). Among the three putative enhancer regions, only E2 showed activation that was dependent on FOXO1 (e). Within E2, the E2-2 subregion was activated by FOXO1 (f). FOXO1 (HR), a DNA binding-deficient form of FOXO1 caused by converting the histidine 212 residue to arginine, failed to activate E2-2 (g). Within E2-2, the E2-2-1 subregion was activated by FOXO1, but not FOXO1 (HR) (h). Mutations disrupting the binding motifs in both sites reduced the activity of E2-2-1 (i).

Supplementary Fig. 6

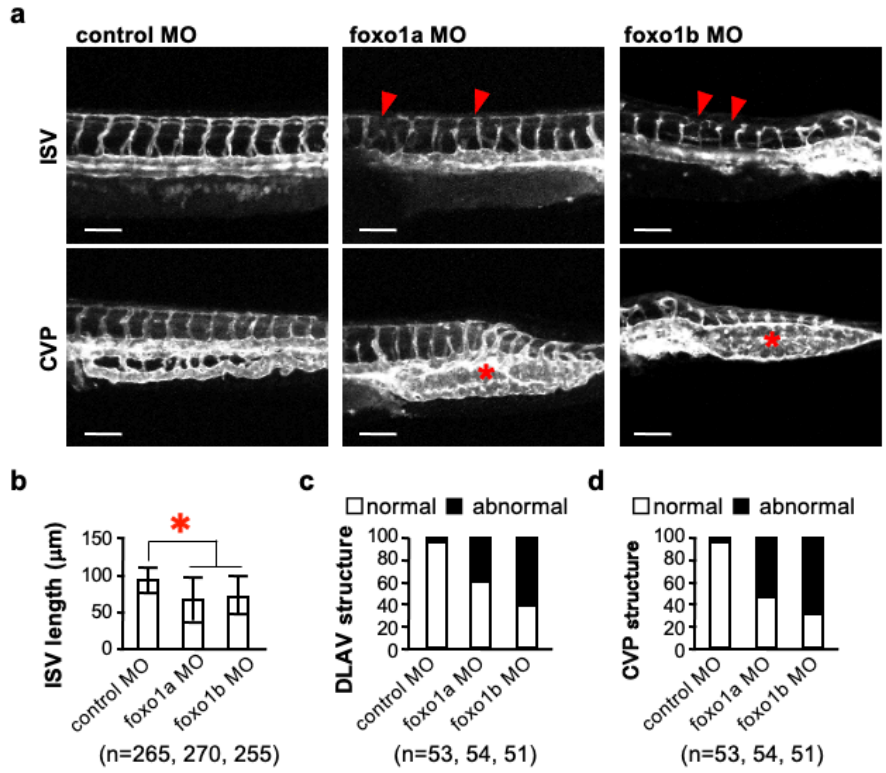

Supplementary Fig. 6 The knockdown of *foxo1a* or *foxo1b* causes an abnormal vascular structure in zebrafish embryos.

Tg(fli1a:Myr-mCherry) zebrafish embryos were injected with foxo1a MO (foxo1a MO) or foxo1b MO (foxo1b MO) (15 ng). (a) The structures of ISV (upper panels) and CVP (lower panels) were analyzed in 2 dpf embryos. Red arrowheads indicate hypoplastic DLAV, and asterisks indicate an incompletely remodeled CVP. Scale bars indicate 100 μm. Similar results were obtained in three independent experiments. (b) The length of ISVs in the morphants. Results were analyzed using Tukey's test (*P<0.05). The total number of ISVs examined in three independent experiments is indicated in the brackets. (c) The ratio of embryos with normal and abnormal DLAV. (d) The ratio of embryos with normal and abnormal CVP. The total number of embryos examined in three independent experiments is indicated in the brackets (c and d).

Supplementary Fig. 7

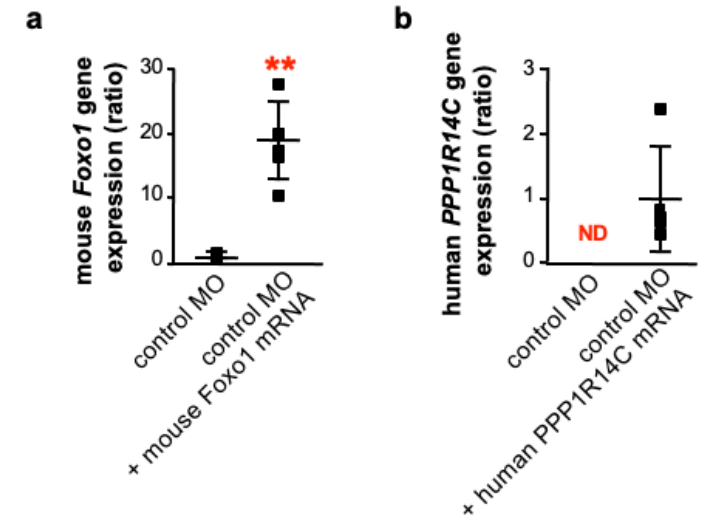

Supplementary Fig. 7 *Foxo1* and *PPP1R14C* mRNA injected into zebrafish embryos is detectable by PCR. *Tg(fli1a:Myr-mCherry)* zebrafish embryos were injected with control MO (14 or 7 ng) with or without mouse *Foxo1* or human *PPP1R14C* mRNA (400 pg each). Mouse *Foxo1* mRNA (a) and human *PPP1R14C* mRNA (b) in zebrafish embryos at 2 dpf were detected using real-time quantitative PCR. Expression levels were normalized to zebrafish *actb1*. Data are presented as a ratio relative to the control. Results were analyzed by an F-test, followed by an unpaired two-tailed *t* test (n=5 from five independent experiments, $^{**}P<0.01$). The small amount of *Foxo1* amplification detected in the control may be due to the sequence of the mouse *Foxo1* primers that are partially homologous to the zebrafish *foxo1* genes (a). *ND* not detected (b).

Supplementary Fig. 8

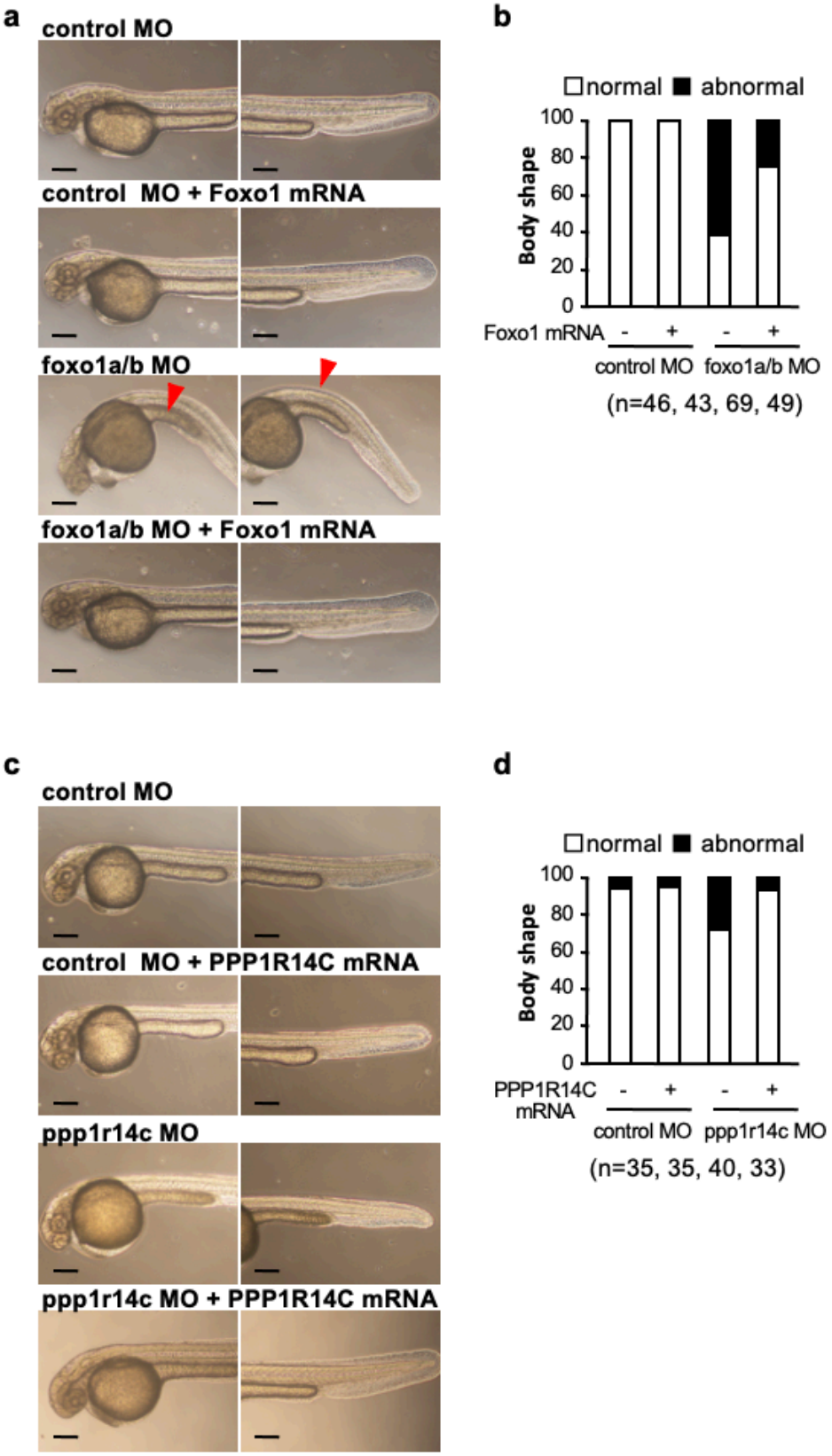

Supplementary Fig. 8 *foxo1*-knockdown causes an abnormal body shape in zebrafish embryos.
Tg(fli1a:Myr-mCherry) zebrafish embryos were injected with control MO (control MO) or a mixture of MO targeting *foxo1a* and *foxo1b* (foxo1a/b MO) (15 ng each, total 30 ng) with or without mouse *Foxo1* mRNA (Foxo1 mRNA) (400 pg) (a and b), or a MO targeting ppp1r14c (ppp1r14c MO) (7 ng) with or without human *PPP1R14C* mRNA (PPP1R14C mRNA) (400 pg) (c and d). (a and c) The representative body shape of 2 dpf embryos. Red arrows indicate bent bodies. Abnormal bent bodies were shown in many of the foxo1a/b morphants (60.9%) or some of the ppp1r14c morphants (27.5%). Scale bars indicate 200 μm. Similar results were obtained in three independent experiments. (b and d) The ratio of embryos with normal and abnormal body shapes. The total number of embryos examined in three independent experiments is indicated in the brackets.

Supplementary Fig. 9

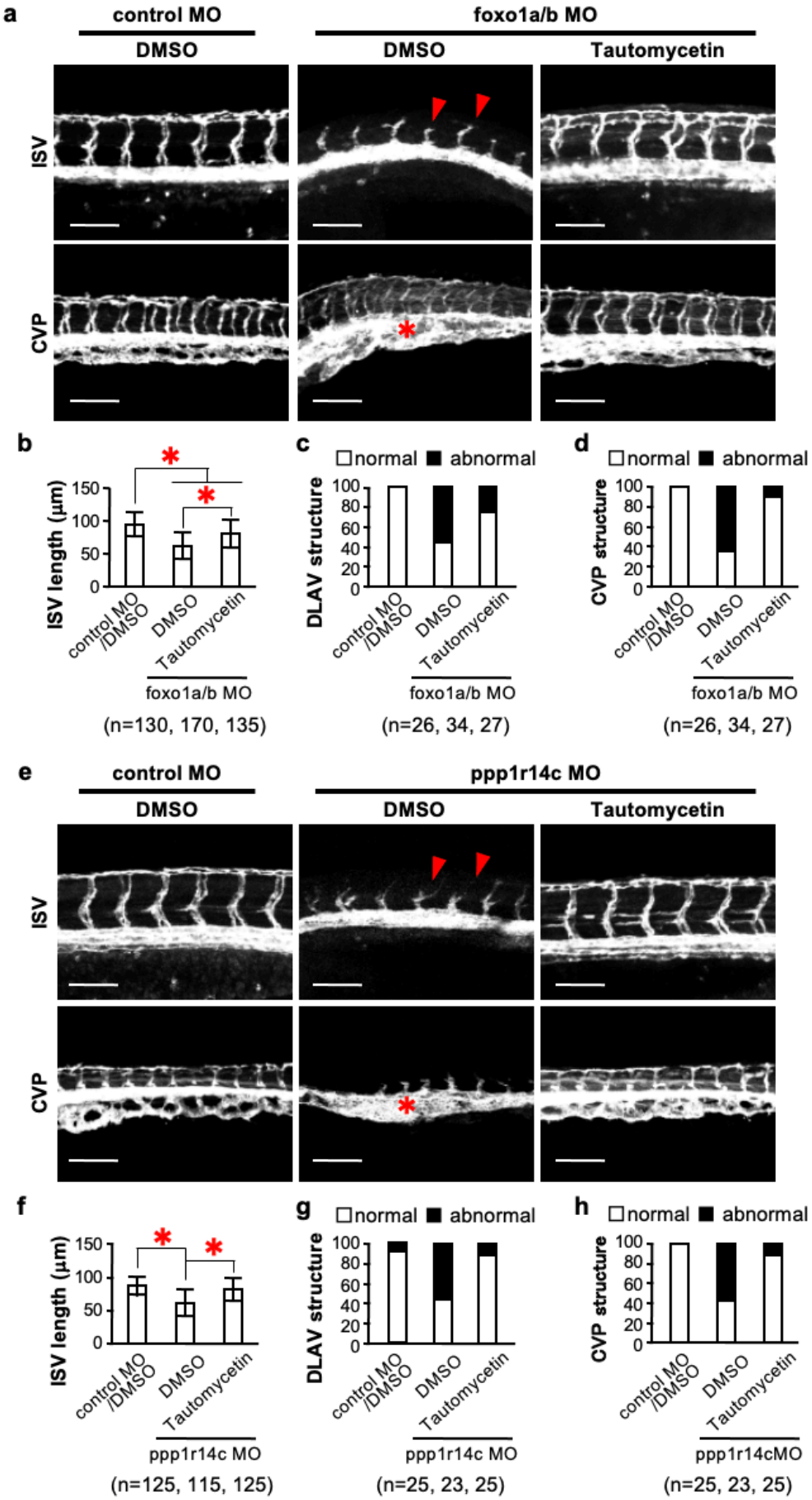

Supplementary Fig. 9 PP1 inhibition by tautomycetin restores vascular defects in *foxo1* or *ppp1r14* morphants. *Tg(fli1a:Myr-mCherry)* zebrafish embryos were injected with a mixture of MO targeting *foxo1a* and *foxo1b* (foxo1a/b MO) (7 ng each, total 14 ng) (a-d) or *ppp1r14c* (ppp1r14c MO) (7 ng) (e-h). The embryos at 6 hpf were exposed to tautomycetin (30 nmol/L). (a and e) The structures of ISVs (upper panels) and CVP (lower panels) were analyzed in 2 dpf embryos. Red arrowheads indicate hypoplastic DLAV, and an asterisk indicates an incompletely remodeled CVP. Scale bars indicate 100 μm. Similar results were obtained in three independent experiments. (b and f) The length of ISVs in the morphants. Results were analyzed using Tukey's test (**P*<0.05). The total number of ISVs examined in three independent experiments is indicated in the brackets. (c and g) The ratio of embryos with normal and abnormal DLAV. (d and h) The ratio of embryos with normal and abnormal CVP. The total number of embryos examined in three independent experiments is indicated in the brackets (c, d, and g, h).

Supplementary Fig. 10

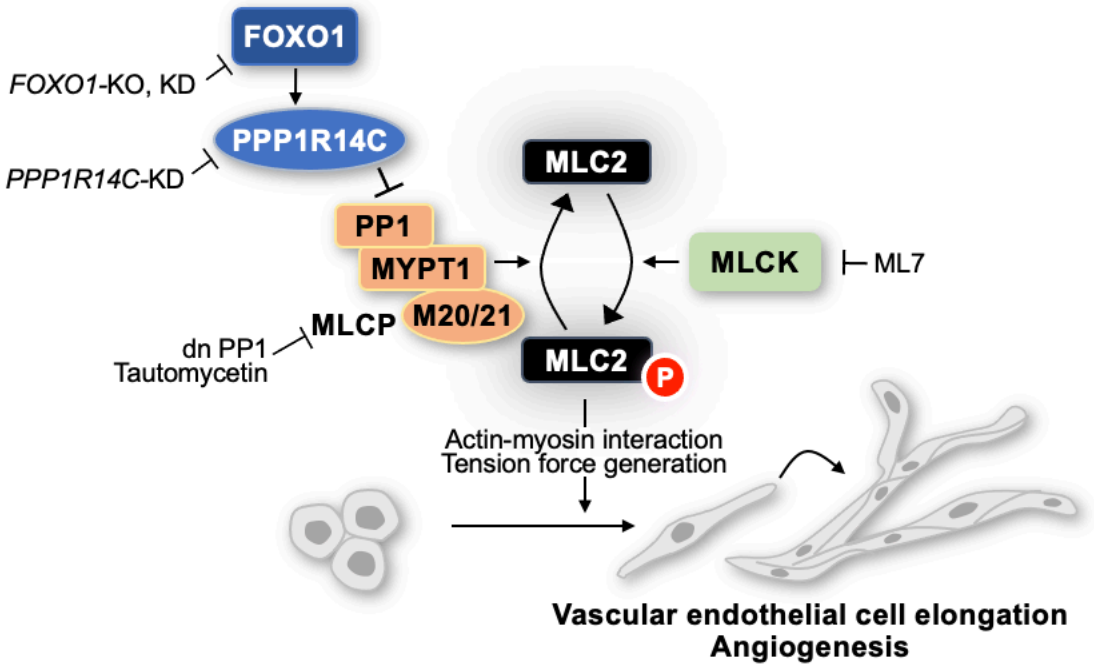

Supplementary Fig. 10 Schematic model of the regulation of endothelial cell elongation by FOXO1 through the phosphorylation of MLC2.

Endothelial cell elongation requires the phosphorylation of MLC2. MLCK catalyzes the phosphorylation of MLC2. In contrast, MLCP, a heterotrimeric complex consisting of PP1, MYPT1, and M20/21, dephosphorylates pMLC2. FOXO1 up-regulates the transcription of the *PPP1R14C* gene. PPP1R14C inhibits PP1 activity, leading to the inactivation of MLCP and an increase in MLC2 phosphorylation. The resulting actin-myosin interaction generates tension, which may propel endothelial cell elongation and angiogenesis. Target molecules for knockout (KO), knockdown (KD), dominant-negative forms (dn), and chemical inhibitors used in the present study are included in the scheme.

Supplementary Table 1. Endothelial cell elongation-related genes (ERG) with a log2 fold change (LogFC) <-0.6 in differentially expressed genes

	Gene_Symbol	logFC [Foxo1(-/-), VEGF(-)] /[Foxo1(+/+), VEGF(+)]	logFC [Foxo1(+/+), VEGF(-)] /[Foxo1(+/+), VEGF(+)]	logFC [Foxo1(-/-), VEGF(+)] /[Foxo1(+/+), VEGF(+)]	Ensembl_Gene_ID
#	Foxo1	-2.769	0.579	-3.840	ENSMUSG00000044167
	Abcb6	-1.387	-1.586	-0.706	ENSMUSG00000026198
	Abcg1	-1.102	-0.967	-0.919	ENSMUSG00000024030
	Acaca	-1.320	-1.307	-0.600	ENSMUSG00000020532
	Acp5	-2.140	-2.374	-1.190	ENSMUSG00000001348
	Acss1	-1.408	-1.544	-0.661	ENSMUSG00000027452
	Adamts14	-1.237	-1.391	-0.655	ENSMUSG00000059901
	Add2	-2.244	-2.660	-1.210	ENSMUSG00000030000
	Adi1	-0.899	-0.842	-1.110	ENSMUSG00000020629
	Adk	-1.187	-1.259	-0.866	ENSMUSG00000039197
	Adra2a	-1.347	-1.181	-1.080	ENSMUSG00000033717
	Ak3l1	-1.353	-1.124	-0.625	ENSMUSG00000028527
	Aldh1a7	-1.339	-1.807	-1.220	ENSMUSG00000024747
	Alox5	-1.881	-1.519	-0.642	ENSMUSG00000025701
	Ankrd27	-1.383	-1.340	-0.831	ENSMUSG00000034867
	Ankrd41	-1.979	-2.348	-0.627	ENSMUSG00000046295
	Ankrd6	-0.980	-1.603	-1.180	ENSMUSG00000040183
	Ankrd9	-1.176	-1.320	-0.997	ENSMUSG00000037904
	Ap4e1	-1.006	-0.820	-0.972	ENSMUSG00000001998
	Aqp8	-1.525	-1.431	-1.110	ENSMUSG00000030762
	Arid2	-1.569	-1.412	-0.625	ENSMUSG00000033237
	Ars2	-2.062	-1.866	-0.614	ENSMUSG00000037364
	Arvcf	-0.666	-0.720	-0.754	ENSMUSG00000000325
	Asb17	-1.472	-1.342	-1.540	ENSMUSG00000038997
	Atf7	-0.976	-1.077	-0.744	ENSMUSG00000052414
	Atp13a3	-1.439	-0.972	-0.777	ENSMUSG00000022533
	Atp1b2	-0.965	-0.679	-0.716	ENSMUSG00000041329
	Atpbd1c	-0.858	-0.866	-0.628	ENSMUSG00000029464
	Atr	-1.634	-1.514	-0.618	ENSMUSG00000032409
	Bdh1	-1.564	-1.703	-0.824	ENSMUSG00000046598
	Blvrb	-1.324	-1.541	-0.774	ENSMUSG00000040466
	Bnip3l	-3.527	-3.588	-0.891	ENSMUSG00000022051
	Brca1	-1.536	-1.893	-0.627	ENSMUSG00000017146
	Bub1	-1.636	-1.686	-0.600	ENSMUSG00000027379
	C9	-1.043	-0.933	-0.659	ENSMUSG00000022149
	Cabp2	-0.781	-0.699	-0.763	ENSMUSG00000024857
	Calr4	-0.742	-0.862	-0.661	ENSMUSG00000028558
	Car1	-1.734	-1.724	-1.320	ENSMUSG00000027556
	Car12	-1.081	-1.432	-1.660	ENSMUSG00000032373
	Ccl25	-0.767	-0.878	-0.608	ENSMUSG00000023235
	Ccr8	-1.949	-1.823	-0.634	ENSMUSG00000042262
	Cdh1	-1.013	-0.866	-0.739	ENSMUSG00000000303
	Cetn4	-0.946	-0.863	-0.609	ENSMUSG00000045031
	Cldn13	-1.581	-2.182	-1.230	ENSMUSG00000008843
	Coch	-0.645	-0.745	-0.706	ENSMUSG00000020953
	Cox6b2	-2.166	-1.993	-1.150	ENSMUSG00000051811
	Cpox	-3.848	-3.769	-1.020	ENSMUSG00000022742
*	Ctse	-1.598	-0.941	-1.020	ENSMUSG00000004552
	Cxcr4	-1.145	-0.970	-0.720	ENSMUSG00000045382
	Cyp46a1	-1.472	-0.911	-1.230	ENSMUSG00000021259
	Dcbld2	-2.490	-2.495	-1.780	ENSMUSG00000035107
	Dnahc2	-1.268	-0.831	-1.010	ENSMUSG00000005237
	Doc2g	-1.421	-1.316	-0.810	ENSMUSG00000024871
	Dopey2	-0.786	-0.622	-0.611	ENSMUSG00000022946
	Drctnnb1	-0.811	-0.828	-0.621	ENSMUSG00000028995
	Ect2	-1.003	-1.176	-0.634	ENSMUSG00000027699
	Eif2c2	-1.304	-1.388	-0.717	ENSMUSG00000036698
	Ell2	-3.393	-3.258	-1.350	ENSMUSG00000001542
	Eno2	-1.932	-1.400	-1.020	ENSMUSG00000004267
	Eno3	-1.423	-1.120	-0.690	ENSMUSG00000060600
	Enpp1	-0.744	-0.657	-0.698	ENSMUSG00000037370
	Epb4.2	-1.842	-1.805	-0.746	ENSMUSG00000023216
	Ephx2	-0.721	-0.770	-0.804	ENSMUSG00000022040
	Epor	-2.726	-2.802	-0.954	ENSMUSG00000006235
*	Fgf3	-1.450	-0.776	-0.731	ENSMUSG00000031074
	Fkbp6	-0.762	-0.744	-0.863	ENSMUSG00000040013
	Fnbp4	-0.695	-0.630	-0.612	ENSMUSG00000008200
	Foxh1	-1.169	-0.751	-0.976	ENSMUSG00000033837
	Foxp2	-1.137	-1.338	-1.470	ENSMUSG00000029563
	Galk1	-1.093	-1.356	-0.602	ENSMUSG00000020766
	Galnt10	-1.308	-1.522	-0.785	ENSMUSG00000020520
	Gan	-1.749	-1.605	-0.654	ENSMUSG00000052557
	Gata1	-2.302	-2.366	-1.090	ENSMUSG00000031162
	Gcat	-0.829	-0.663	-1.100	ENSMUSG00000006378
	Gcnt1	-2.319	-1.740	-0.946	ENSMUSG00000038843
	Gfpt2	-1.523	-1.134	-0.687	ENSMUSG00000020363
	Gga2	-1.079	-1.209	-0.657	ENSMUSG00000030872
	Gjb3	-1.840	-1.762	-1.050	ENSMUSG00000042367
	Glce	-1.241	-1.352	-0.680	ENSMUSG00000032252
	Glp2r	-0.626	-1.376	-0.806	ENSMUSG00000049928
	Glt28d2	-1.621	-1.451	-0.676	ENSMUSG00000031286
	Gpam	-0.818	-0.771	-0.694	ENSMUSG00000024978
	Grina	-0.729	-0.619	-0.609	ENSMUSG00000022564
	Grtp1	-2.256	-2.250	-0.676	ENSMUSG00000038515
	Gtlf3a	-1.410	-1.131	-0.975	ENSMUSG00000042549
	Gypa	-2.490	-3.028	-1.010	ENSMUSG00000051839
	H2afz	-0.638	-1.415	-0.787	ENSMUSG00000037894
	Hbax	-3.036	-3.719	-0.871	ENSMUSG00000055609
	Hbbb1	-1.821	-2.351	-0.666	ENSMUSG00000052305
	Hbbbh1	-2.387	-2.639	-0.812	ENSMUSG00000052217
	Hdac11	-1.155	-0.994	-0.621	ENSMUSG00000034245
	Hemgn	-1.258	-1.158	-0.858	ENSMUSG00000028332
	Hk1	-2.363	-2.139	-0.961	ENSMUSG00000037012
	Hk2	-1.049	-0.846	-0.852	ENSMUSG00000000628
	Homer2	-1.657	-1.699	-1.100	ENSMUSG00000025813
	Hsd3b6	-0.781	-1.173	-1.120	ENSMUSG00000027869
	Hsp110	-1.239	-1.116	-0.690	ENSMUSG00000029657
	Htra1	-0.770	-0.772	-0.613	ENSMUSG00000006205
	Icam4	-1.481	-1.368	-1.140	ENSMUSG00000001014
	Igsf3	-1.758	-1.313	-1.000	ENSMUSG00000042035
	Itsn2	-0.859	-1.241	-0.626	ENSMUSG00000020640
	Ivd	-1.140	-1.536	-0.652	ENSMUSG00000027332
	Kcnn4	-3.183	-3.200	-1.280	ENSMUSG00000054342
	Kctd1	-0.621	-0.696	-0.707	ENSMUSG00000036225
	Kel	-1.422	-1.346	-0.979	ENSMUSG00000029866
	Klf1	-3.164	-3.298	-1.100	ENSMUSG00000054191

	Klhl12	-1.227	-1.075	-0.774	ENSMUSG00000026455
*	Lgr5	-1.440	-0.812	-0.933	ENSMUSG00000020140
	Lig1	-0.606	-0.933	-0.700	ENSMUSG00000056394
	Liph	-1.266	-1.050	-0.639	ENSMUSG00000044626
	Llgl2	-0.924	-0.696	-0.820	ENSMUSG00000020782
	Mafk	-0.898	-0.708	-0.658	ENSMUSG00000018143
	Matn1	-2.433	-2.300	-1.570	ENSMUSG00000040533
	Mbl2	-0.832	-0.744	-0.623	ENSMUSG00000024863
	Mcf2	-0.844	-1.053	-0.606	ENSMUSG00000031139
	Med12l	-1.550	-1.450	-0.612	ENSMUSG00000056476
	Mgst3	-1.138	-1.585	-0.698	ENSMUSG00000026688
*	Mkx	-3.137	-2.443	-1.760	ENSMUSG00000061013
	Mll5	-0.628	-0.735	-0.683	ENSMUSG00000029004
	Mllt3	-1.669	-2.270	-0.618	ENSMUSG00000028496
	Mpp2	-2.410	-2.283	-0.825	ENSMUSG00000017314
	Mrm1	-1.632	-1.668	-0.695	ENSMUSG00000018405
	Msh6	-1.321	-1.535	-0.794	ENSMUSG00000005370
	Mtmr3	-1.044	-1.411	-0.661	ENSMUSG00000034354
	Mybbp1a	-0.896	-0.989	-0.712	ENSMUSG00000040463
	Mybpc3	-1.033	-0.661	-0.969	ENSMUSG00000002100
	Myc	-0.667	-0.795	-0.728	ENSMUSG00000022346
	Mycs	-0.873	-1.276	-0.856	ENSMUSG00000044597
	Myo9a	-1.032	-1.556	-0.848	ENSMUSG00000039585
*	Nanog	-2.418	-1.580	-1.020	ENSMUSG00000012396
	Ndrg2	-1.963	-1.554	-0.693	ENSMUSG00000004558
	Nmnat3	-2.178	-2.448	-0.767	ENSMUSG00000032456
	Nrip3	-1.308	-1.055	-1.060	ENSMUSG00000034825
	Nt5c2	-1.402	-1.450	-0.656	ENSMUSG00000025041
	Olfm1	-1.912	-1.718	-1.210	ENSMUSG00000026833
	Olfr1360	-0.748	-0.869	-0.824	ENSMUSG00000056866
	Olfr346	-1.455	-0.976	-0.754	ENSMUSG00000063915
	Olfr376	-1.802	-2.292	-0.977	ENSMUSG00000063881
	Olfr463	-0.604	-0.657	-0.690	ENSMUSG00000058075
	Olfr486	-0.868	-1.208	-0.760	ENSMUSG00000063610
	Olfr690	-0.814	-0.836	-0.627	ENSMUSG00000050266
	Olfr823	-1.725	-1.224	-0.831	ENSMUSG00000060564
	Olfr933	-0.691	-0.862	-0.635	ENSMUSG00000058515
	Orc1l	-0.703	-0.858	-0.816	ENSMUSG00000028587
	Osbpl3	-0.640	-0.870	-0.705	ENSMUSG00000029822
*	Oxsr1	-1.380	-0.647	-0.768	ENSMUSG00000036737
	Pabpc4	-1.123	-0.979	-0.681	ENSMUSG00000011257
	Pcx	-0.962	-1.092	-0.962	ENSMUSG00000024892
	Pdcd4	-1.308	-1.552	-0.700	ENSMUSG00000024975
	Pfkfb4	-1.890	-2.280	-0.792	ENSMUSG00000025648
	Pfkl	-2.082	-2.173	-0.624	ENSMUSG00000020277
	Pigw	-0.690	-0.800	-0.612	ENSMUSG00000045140
	Pim1	-3.017	-3.076	-0.606	ENSMUSG00000024014
	Pip5k1a	-1.528	-1.648	-0.861	ENSMUSG00000024867
	Pkm2	-2.289	-2.354	-1.480	ENSMUSG00000032294
	Plod2	-1.576	-1.366	-0.784	ENSMUSG00000032374
	Pml	-1.134	-1.221	-0.603	ENSMUSG00000036986
	Pnpo	-1.562	-1.656	-0.693	ENSMUSG00000018659
	Pofut1	-1.144	-1.368	-0.701	ENSMUSG00000046020
	Ppcs	-0.680	-0.749	-0.764	ENSMUSG00000028636
	Ppox	-2.925	-2.784	-0.710	ENSMUSG00000062729
	Ppp1r13l	-0.978	-0.731	-0.812	ENSMUSG00000040734
	Ppp1r14c	-1.462	-1.223	-0.752	ENSMUSG00000040653
	Prkag2	-0.990	-1.017	-0.621	ENSMUSG00000028944
	Prokr1	-0.853	-1.030	-1.100	ENSMUSG00000049409
	Prr6	-1.515	-1.670	-0.952	ENSMUSG00000018509
	Qsox6l1	-0.690	-1.084	-0.787	ENSMUSG00000036327
	Rab33a	-1.529	-1.954	-0.927	ENSMUSG00000031104
	Rad50	-1.206	-1.664	-0.763	ENSMUSG00000020380
	Rbm3	-2.755	-2.806	-0.895	ENSMUSG00000031167
	Rbm35a	-1.599	-2.091	-1.360	ENSMUSG00000040728
	Reep6	-2.344	-2.122	-1.130	ENSMUSG00000035504
	Rev1l	-1.053	-1.228	-0.649	ENSMUSG00000026082
	Rgs11	-1.349	-1.265	-1.240	ENSMUSG00000024186
	Rhag	-3.634	-3.199	-1.670	ENSMUSG00000023926
	Rhd	-2.143	-2.531	-1.850	ENSMUSG00000028825
	Rlf	-1.483	-1.533	-0.617	ENSMUSG00000049878
	Rnf19	-0.690	-0.922	-0.793	ENSMUSG00000022280
	Rpia	-2.636	-2.494	-0.925	ENSMUSG00000053604
	Scin	-0.817	-1.057	-0.747	ENSMUSG00000002565
	Serpinb1	-0.678	-0.684	-0.831	ENSMUSG00000048775
	Slc15a2	-2.130	-1.903	-0.929	ENSMUSG00000022899
	Slc16a6	-1.906	-1.933	-1.270	ENSMUSG00000041920
	Slc19a2	-0.627	-0.925	-0.694	ENSMUSG00000040918
	Slc25a37	-3.760	-3.919	-1.370	ENSMUSG00000034248
	Slc29a2	-1.429	-1.375	-0.732	ENSMUSG00000024891
	Slc2a3	-1.581	-1.028	-0.843	ENSMUSG00000003153
*	Slc30a10	-3.331	-2.728	-1.270	ENSMUSG00000026614
	Slc35f2	-1.466	-1.655	-0.800	ENSMUSG00000042195
	Slc38a5	-2.176	-2.383	-1.370	ENSMUSG00000031170
	Slc39a8	-1.943	-1.759	-1.380	ENSMUSG00000053897
	Slc7a4	-0.691	-0.905	-0.757	ENSMUSG00000022756
	Smox	-2.165	-2.162	-0.780	ENSMUSG00000027333
	Snca	-1.983	-2.184	-0.957	ENSMUSG00000025889
	Snx9	-0.967	-0.992	-0.760	ENSMUSG00000002365
	Spink3	-2.171	-1.651	-2.410	ENSMUSG00000024503
	Spnb1	-2.806	-2.739	-0.904	ENSMUSG00000021061
	Sprr2i	-1.124	-1.081	-0.610	ENSMUSG00000042157
	Ssx2ip	-1.683	-1.717	-1.080	ENSMUSG00000036825
	Stat5b	-1.093	-1.003	-0.673	ENSMUSG00000020919
	Suv420h2	-0.949	-0.859	-0.809	ENSMUSG00000059851
	Taf4b	-0.786	-0.673	-0.832	ENSMUSG00000054321
	Tbxas1	-1.754	-1.870	-0.725	ENSMUSG00000029925
	Tcfap2c	-2.358	-1.902	-1.080	ENSMUSG00000028640
	Tdh	-1.613	-1.447	-1.200	ENSMUSG00000021953
	Tef	-0.970	-0.910	-0.794	ENSMUSG00000022389
	Tkt	-0.795	-0.952	-0.737	ENSMUSG00000021957
	Tm2d3	-1.031	-1.066	-0.723	ENSMUSG00000030515
	Tmem16a	-1.065	-1.067	-0.886	ENSMUSG00000031075
	Tmod1	-2.024	-1.946	-0.893	ENSMUSG00000028328
	Tspan33	-2.143	-2.447	-1.410	ENSMUSG00000001763
	Tst	-2.099	-1.613	-0.635	ENSMUSG00000044986
	Tuft1	-1.817	-1.873	-0.946	ENSMUSG00000005968
	Ube2l6	-1.024	-0.902	-0.713	ENSMUSG00000027078
	Ube2t	-1.076	-1.144	-0.617	ENSMUSG00000026429
	Uros	-1.294	-1.532	-1.010	ENSMUSG00000030979
	V1rh15	-1.010	-1.290	-0.870	ENSMUSG00000057209
*	Vtcn1	-1.525	-0.842	-0.757	ENSMUSG00000051076

	Vwa1	-0.869	-1.359	-0.995	ENSMUSG00000042116
	Wapal	-1.705	-1.789	-0.710	ENSMUSG00000041408
	Wdfy3	-1.008	-1.730	-0.704	ENSMUSG00000043940
	Xtrp3s1	-0.947	-1.440	-0.748	ENSMUSG00000036814
*	Ythdc2	-1.706	-0.744	-1.230	ENSMUSG00000034653
	Zdhhc14	-1.039	-0.943	-0.851	ENSMUSG00000034265
	Zfp719	-0.644	-0.678	-0.686	ENSMUSG00000030469
	Zfp75	-1.653	-1.724	-0.676	ENSMUSG00000057551
	Zfp98	-0.637	-0.830	-1.050	ENSMUSG00000030380

[Foxo1(-/-), VEGF(-)], Foxo1-/- embryonic stem cell (ESC)-derived vascular endothelial cells (ECs) cultured without VEGF; [Foxo1(+/+), VEGF(+)], Foxo1+/+ ESC-derived ECs cultured with VEGF; [Foxo1(+/+), VEGF(-)], Foxo1+/+ ESC-derived ECs cultured without VEGF; [Foxo1(-/-), #*Foxo1* is shown as a reference of its deficiency.
* Genes common to Supplementary Table 1 and 3.